論文 / 著書情報
Article / Book Information

題目(和文)	皮質脳波を用いた上肢ブレインーマシンーインタフェース
Title(English)	Upper limb brain machine interface based on electrocorticography signals
著者(和文)	陳超
Author(English)	chao chen
出典(和文)	学位:博士(学術), 学位授与機関:東京工業大学, 報告番号:甲第9600号, 授与年月日:2014年6月30日, 学位の種別:課程博士, 審査員:小池　康晴,佐藤　誠,熊澤　逸夫,中村　健太郎,金子　寛彦
Citation(English)	Degree:Doctor (Academic), Conferring organization: Tokyo Institute of Technology, Report number:甲第9600号, Conferred date:2014/6/30, Degree Type:Course doctor, Examiner:,,,,
学位種別(和文)	博士論文
Type(English)	Doctoral Thesis

Upper limb brain machine interface based on electrocorticography signals

(皮質脳波を用いた上肢ブレイン–マシン–インタフェース)

Department of Information Processing

Chen Chao

Acknowledgments

It would not have been possible to finish this thesis without the help and support of the kind people around me during almost four years of doctoral study. Here, I would like to express sincere gratitude to these people.

I would like to thank Dr. Keiji Uchikawa who introduced me to Koike laboratory when I was a research student in his laboratory.

I would like to thank my academic supervisor Dr. Yasuharu Koike, who provided insightful guidance at each phase of doctoral study, and encouraged me when I met some difficulties in research works. In addition, He also showed concern about my daily life and helped me to apply financial support from Monbukagakusho.

I would like to thank Duk Shin, PhD who gave me important initial guidance about the whole process of completing a good journal paper, taught me many technology details and precious experiences in both academic and daily life.

I would like to thank Dr. Hiroyuki Kambara, Dr. Natsue Yoshimura, Dr. Yasuhiko Nakanishi, and the staff Ryoko Sasaki for the meaningful discussion about research, and the support of daily life in Koike laboratory.

I would like to thank Tadashi Isa, PhD, Yukio Nishimura, PhD, and Hidenori Watanabe, PhD at National Institute for Physiological Sciences for their efforts in providing the experimental date and valuable discussion and comments in this study.

I would like to thank the members of my PhD committee, Dr. Makoto Sato, Dr. Kentaro Nakamura, Dr. Itsuo Kumazawa, and Dr. Hirohiko Kaneko for reviewing this thesis and providing valuable comments.

I would like to thank Dr. C. S. DaSalla for proofreading the manuscript of this thesis.

Finally, I would like to thank my parents and my wife for their love and encouragement during all these years.

Abstract

Over the past two decades, brain-machine interfaces (BMI) have been developed utilizing the growing understanding of brain function and the development of technology to measure brain activity. BMIs are mainly categorized into two types, invasive and non-invasive BMIs, according to the signal source.

As semi-invasive brain signals, electrocorticography (ECoG) has received much focus in recent years. ECoG signals have higher signal-to-noise ratio and spatiotemporal resolution than non-invasive recording methods. In addition, long-term stability had been showed and the level of clinical risk is lower compared with invasive methods.

The goal of this study is to develop a high performance ECoG-based upper limb brain machine interface, such as self-feeding robot. To accomplish this goal, position information and grasp force in time series are necessary. Three-dimensional hand positioning, grasp force, and ECoG signals of the primary motor cortex (Ml), were recorded simultaneously in two Japanese monkeys while they performed reaching and grasping tasks.

Raw ECoG signals were common average referenced and band-pass filtered using ten different sensorimotor frequency band-pass filters to select motor related feature in ECoG signals. A partial least square linear regression method was applied to decode hand trajectory from ECoG feature signals. Decoding results indicated that 3D hand trajectories can be predicted using nine or ten ECoG electrodes and ECoG electrodes with higher performance were concentrated at the lateral areas and areas

close to the central sulcus (CS). Likewise, it is also demonstrated that lateral grasp force profile can be decoded using a sparse linear regression from ECoG feature signals.

In addition, the future directions of brain research and interface development were investigated. The major burns in current brain research and interface development were discussed. With the development of next generational ECoG electrode, ECoG signals may play an important role in future brain and interface research.

In the end, the feasibility to realize real time robot control was analyzed and discussed, based on these results. On-line validation and experiments on human subjects are considerable work in the future.

Table of Contents

1 Introduction **9**
1.1 brain machine interface **9**
1.2 invasive, no invasive and semi-invasive BMI **10**
1.3 The goal of this study **11**
1.4 Structure of this thesis **12**
2 Related research and methods based on ECoG signals **14**
2.1 Related research ECoG works **14**
2.2 Decoding algorithm in this study **16**
2.2.1 Partial least square regression 16
2.2.2 Sparse linear regression 18
3 Prediction of hand trajectory from ECoG signals **20**
3.1 Introduction **20**
3.2 Methods **23**
3.2.1 Ethics statement 23
3.2.2 Behavioral Task 23
3.2.3 Preprocessing and feature selection 26
3.2.4 Partial Least Squares Regression 28
3.2.5 Two methods for electrode selection 29
3.2.6 Analysis 30
3.3 Result **33**
3.3.1 Prediction with the location-based selection method 33
3.3.2 Prediction with the performance-based selection method 40
3.3.3 Summary of the two electrode selection methods 42
3.3.4 Analysis of specific frequency bands 45
3.4 Discussion **48**
3.4.1 main work in this study 48
3.4.2 Which locations are most effective for prediction? 48
3.4.3 How did different numbers of ECoG electrodes affect performance? 48
3.4.4 Which frequency bands are most effective? 49
4 Prediction of grasp force profile from ECoG signals **51**

4.1 Introduction **51**
4.2 Method **53**
4.2.1 Ethics statement 53
4.2.2 Monkey subjects and experimental procedure 53
4.2.3 ECoG and force data collection 53
4.2.4 Decoding algorithm and data analysis 54
4.3 Result **59**
4.3.1 Decoding results of lateral grasp force profile 59
4.3.2 Contribution of individual electrodes and frequency bands to decoding 63
4.4 Discussion **66**
5 Perspective of brain research and interface development with ECoG signals **69**
5.1 Developments of next generational ECoG **69**
5.2 Future brain research with ECoG signals **69**
5.2.1 Major obstacles in brain research 69
5.2.2 Brain research with next generational ECoG signals 71
5.3 Future brain machine interface development with ECoG signals **73**
6 Conclusion **75**
6.1 Summary **75**
6.2 Future work **76**
Reference **79**
Research achievement **90**

List of Figures

Figure 1-1. Robot control using brain activity 9
Figure 1-2. Three types of brain machine interface 10
Figure 3-1. Behavioral task and location of ECoG electrodes used in decoding 24
Figure 3-2. Example of measured trajectory and frequency band feature data during a movement task 28
Figure 3-3. Predictive error sum of squares in model training for monkey A 31
Figure 3-4. Predictive error sum of squares in model training for monkey B 32
Figure 3-5. Decoding results using 32 electrodes selected with the location-based method for monkey B 34
Figure 3-6. Decoding result of monkey B in three dimensional space 35
Figure 3-8. Decoding results for monkey A in three dimensional space 37
Figure 3-9. Decoding results for monkey B with different electrode numbers selected using the location-based method 38
Figure 3-10. Decoding results for monkey A with different electrode numbers selected using the location-based method 39
Figure 3-11. Decoding result form each electrode and performance details of two methods. 41
Figure 4-1. ECoG electrode locations 54
Figure 4-2. ECoG spectral feature and raw force data 55
Figure 4-3. Sample of predicted force profile 60
Figure 4-4. Histogram of whole result in 10-fold cross validation 62
Figure 4-5. Contribution of electrodes 65
Figure 4-6. Contribution of frequency bands 65
Figure 5-1. Design of wireless ECoG electrode 69
Figure 5-2. From molecules to the body: spatial scales for the brain's different levels of organization span nine orders of magnitude 71
Figure 5-3. Decoding performances with individual ECoG electrodes 72

List of Tables

Table 2-1. Summary of related ECoG based brain machine interface researches ... 15
Table 3-1. Prediction results using location-based electrode selection in the rostral-caudal direction ... 44
Table 3-2. Prediction results using location-based electrode selection in the medial-lateral direction ... 44
Table 3-3. Prediction results using individual frequency bands ... 47
Table 4-1. Decoding performances of 10-fold cross validation for both monkeys ... 61

Chapter 1

Introduction

1.1 brain machine interface

Every year, hundreds of thousand people became amputees caused by traffic accidents, or suffer from severe neurological disease such as amyotrophic laterals clerosis (ALS), spinal cord injury, brain stroke and cerebral paralysis. Brain machine interface can help these people to communicate with outside, operate computer cursors, control wheelchair or robot arms (Figure 1-1), by using their neural activities.

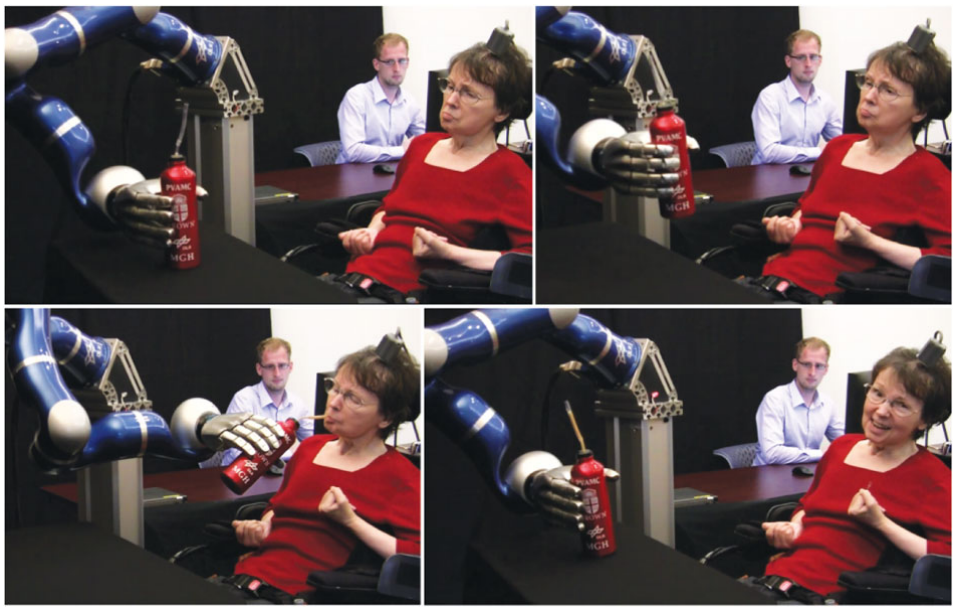

Figure 1-1. Robot control using brain activity

This figure is from Hochberg et al., 2012

For brain research, studies on brain machine interface continue to offer an important insight into how three-dimensional external word represents in the brain, how brain plan and control movement, and how neurons and their connections change

with feedback from the usage of brain machine interface.

1.2 invasive, no invasive and semi-invasive BMI

According to recording location and invasiveness of the measurement of brain signals, BMI were divided into three types: invasive, noninvasive and semi-invasive BMI, as shown in Figure 1-2.

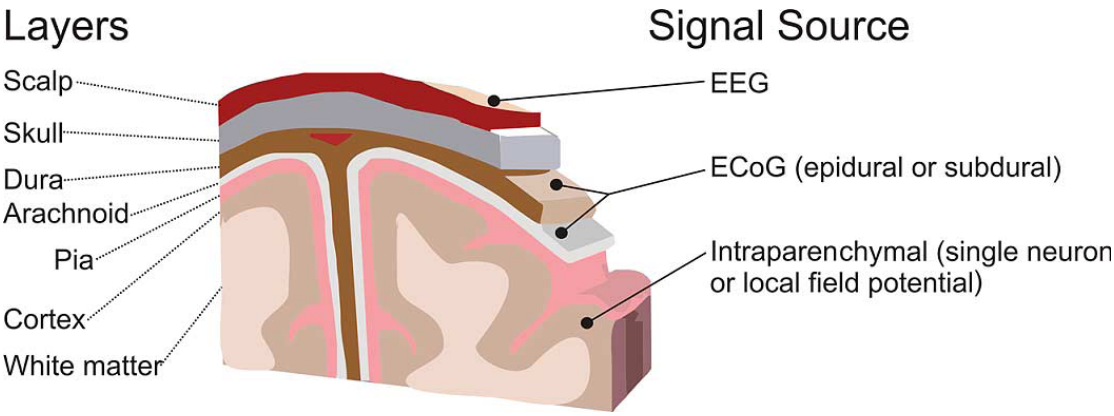

Figure 1-2. Three types of brain machine interface

This figure is from Schalk et al., 2011

Invasive methods penetrate the cortex to record single neuron spike activity (SNA), or local field potentials (LFPs). SNA based BMI, a typical invasive BMI, which measure activities form cortical neurons directly has high spatial resolution and signal-to-noise rate. Kinematic information can be decoded in real time and used for on-line robot control in SNA based BMI. Muscle activities in time series also can be reconstructed in our previous SNA study. Because of penetration of brain, invasive BMI suffer from high clinical risk and poor long-term stability. Although human subject joined invasive BMI research (Hochberg et al., 2006,

Hochberg et al., 2012, and Collinger et al., 2013), high clinical risk is still the major burden for practical clinical solution.

On the other hand, EEG based BMI, which record brain signals from the scalp, was widely used in human subjects as a safety no-invasive BMI. It provided basic communication to people with severe disability, however, the low spatial resolution and ambiguous in high frequency reduce information capacity with EEG signals, compared with invasive signals. It is still difficult to realized three-dimensional movement control of robot arm or neural prosthetic by using EEG signals. In addition, functional magnetic resonance imaging (fMRI), which measures the tiny metabolic changes of active part of the brain, and magnetoencephalography (MEG), which records magnetic fields produced by electrical currents occurring naturally in the brain, are common noninvasive recording methods.

Since the limitation in both invasive and no-invasive BMI, as semi-invasive brain signals, electrocorticographic (ECoG) signals have been in focus during recently years. ECoG electrodes were placed on the surface of brain, subdural or epidural. ECoG signals have high signal noisy rate, spatial-temporal resolution. Recent researches showed ECoG signals are potential to support high performance neural prosthetics with high degrees of freedom.

1.3 The goal of this study

The goal of this study is to develop a high performance ECoG-based upper limb brain machine interface for supporting robot arm or prosthetic with multi-degree of freedom. To accomplish this goal, we trained two Japanese monkeys to perform reaching and grasping tasks. Three-dimensional hand positioning, grasp force, and

ECoG signals of the primary motor cortex (Ml), were recorded simultaneously in reaching and grasping tasks. Then, we decoded hand trajectory and grasp force profile in time series from ECoG signals. As future work, we want to realize real time robot control based on these results.

1.4 Structure of this thesis

In chapter 1, the background of brain machine interface was described, including the history and motivation of brain machine interface research. Then, three typical type brain machine interface: invasive, noninvasive, and semi-invasive BMI, were introduced. Based on mentioned fundamental knowledge, the goal of this study was proposed. Structure of this thesis was at end of this chapter.

In chapter 2, the contents and methods in related ECoG based BMI researches were reviewed to show the position of this study in this research field. Then, the feature selection and prediction methods in this study were introduced and compared with related methods.

In chapter 3, the hand trajectory was predicted from ECoG signals in primary motor cortex. At the beginning, behavioral tasks and data measurement of ECoG signals and three-dimensional positions were introduced. Then, the partial least square regression method, two electrode selection methods, and data analysis method were described. The prediction results showed that three-dimensional hand trajectories can be predicted using nine or ten ECoG signals and that ECoG electrodes with higher performance were concentrated at the lateral areas and areas close to the central sulcus.

In chapter 4, the grasp force profile was decoded from ECoG signals in primary motor cortex. Brief description was held on behavioral tasks and experimental procedure, signal-processing method to ECoG signals and detection of grasp force profile. Then, a sparse linear regression method was employed to predict the grasp force profile. Results showed grasp force profile could be decoded from ECoG signals and the efficacy of high γ bands in decoding.

In chapter 5, current research projects in brain research were introduced. Then, the main issues in brain and interface research were reviewed. Finally, combined with the result gotten in this study, the potential future solutions of brain and interface research with ECoG signals were discussed.

In chapter 6, the main works in this study were summarized. As a future vision, ECoG based research may be become a key point in brain and interface research.

Chapter 2

Related research and methods based on ECoG signals

2.1 Related research ECoG works

Initially, ECoG electrodes were implanted to treat intractable head pain or epilepsy. With the growing interest in BMI research, some patients joint the experiment depends on their willing in the duration of about two weeks monitoring. The first online ECoG based BMI were developed by Leuthardt et al. in human subjects. Electrocorticography (ECoG) has drawn attention as a new type of signal source for BMI. Within about ten years following with this succeed, productive ECoG based BMI research were reported, including cursor control (Leuthardt et al., 2004, Schalk et al., 2008, and Wang et al., 2013), classification of hand movement (Chin et al., 2007, Yanagisawa et al., 2009, and Yanagisawa et al., 2011), and grasp types (Pistohl et al., 2012), detection of start time point of grasp (Pistohl et al., 2013), decoding of muscle activities (Shin et al., 2012), movement-related intracortical activity (Watanabe et al., 2012), hand trajectories (Schalk et al., 2007, Chao et al., 2010, Shimoda et al., 2012, Nakanishi et al., 2013, and Chen et al., 2013) and finger movement (Kubanek et al., 2009 and Acharya et al., 2010) in human and monkey subjects. Typical works were summarized in Table 2-1. In these works, special frequency bands were extracted from ECoG signals by using Fourier transform, Wavelet transform or band-pass filters in feature selection, and linear regression methods were usual methods as decoding methods.

Table 2-1. Summary of related ECoG based brain machine interface researches

Year	Author	Feature selection method	Decoding method
2004	Leuthardt et al	Spectral amplitudes between 0 and 200Hz in 2Hz bins	A weighted, linear summation of the amplitudes in identified frequency bands
2007	Schalk et al	Special frequency band (8–12, 18–24, 35–42, 42–70, 70–100, 100–140, 140–190 Hz)	Auto regression
2007	Chin et al	0-99Hz in 3Hz bins, 0-100Hz in 5 Hz bins, 0-98Hz in 7Hz bins, 0-100Hz in 10Hz bins histograms	Nearest neighbor classifier
2010	Chao et al	Wavelet transform between 10 and 150Hz in 10Hz bins	Partial least square regression
2011	Pistohl et al	Three frequency band: 2-6, 14-46, 54-114Hz	Regularized linear discriminant analysis
2012	Shin et al	Sensorimotor frequency bands (1.5-4, 4-8, 8-12, 12-20, 20-30, 30-50, 50-90Hz)	Sparse linear regression
2012	Watanabe et al	Broadband (1–250 Hz), β band (10–35 Hz), and high-γ band (80–170 Hz)	Sparse linear regression
2012	Shimoda et al	Wavelet transform between 10 and 120Hz in 10Hz bins	Partial least square regression
2013	Pistohl et al	6.7Hz low pass filter, frequency band amplitudes between 0 and 128Hz in 4Hz bins	Regularized linear discriminant analysis

2.2 Decoding algorithm in this study

2.2.1 Partial least square regression

Partial least square regression and sparse linear regression methods were employed to decode hand trajectory and grasp force profile, respectively in this study. Partial least square regression model Y from X, based on the decomposition of Y and X.

Assuming that, Y with m variables and X with n variables have k observations to form k-by-m response matrix and k-by-n matrix of predictor variables, respectively, with rows corresponding to observations, columns to variables. These two matrices were z-score normalized, and denoted as following:

$$F_0 = \begin{bmatrix} y_{11} & \cdots & y_{1m} \\ \vdots & \ddots & \vdots \\ y_{k1} & \cdots & y_{km} \end{bmatrix}, E_0 = \begin{bmatrix} x_{11} & \cdots & x_{1n} \\ \vdots & \ddots & \vdots \\ x_{k1} & \cdots & x_{kn} \end{bmatrix} \quad (1)$$

Then, the details of modeling were described as four steps as following:

Step1: if u_1 and t_1 are linear combination of Y and X, respectively, and defined as $u_1 = v_{11}y_1 + \cdots + v_{1m}y_m = v_1^T Y$ and $t_1 = w_{11}x_1 + \cdots + w_{1n}x_n = w_1^T X$. It is expected that u_1 and t_1 can carry information of Y and X as much as possible, and have largest correlation. It also can be denoted as matrix form, as following:

$$\hat{u}_1 = F_0 v_1 = \begin{bmatrix} y_{11} & \cdots & y_{1m} \\ \vdots & \ddots & \vdots \\ y_{k1} & \cdots & y_{km} \end{bmatrix} \begin{bmatrix} v_{11} \\ \vdots \\ v_{1m} \end{bmatrix} = \begin{bmatrix} u_{11} \\ \vdots \\ u_{k1} \end{bmatrix} \quad (2)$$

$$\hat{t}_1 = E_0 w_1 = \begin{bmatrix} x_{11} & \cdots & x_{1n} \\ \vdots & \ddots & \vdots \\ x_{k1} & \cdots & x_{kn} \end{bmatrix} \begin{bmatrix} w_{11} \\ \vdots \\ w_{1n} \end{bmatrix} = \begin{bmatrix} t_{11} \\ \vdots \\ t_{k1} \end{bmatrix} \quad (3)$$

Because the maximum of covariance $Cov\,(u_1, t_1)$ means the larger correlation between u_1 and t_1, and $Cov\,(u_1, t_1)$ can be calculated by the inner product from $\hat{u}_1$

and $\hat{t}_1$. The question change to calculate the conditional maximum value, as shown in following:

$$\begin{cases} \langle \hat{t}_1,\ \hat{u}_1 \rangle = \langle E_0 w_1, F_0 v_1 \rangle = w_1^T E_0^T F_0 x_1 \Rightarrow max \\ w_1^T w_1 = \|w_1\|^2 = 1,\ v_1^T v_1 = \|v_1\|^2 = 1 \end{cases} \tag{4}$$

With the method of Lagrange multipliers, this question change to calculate unit vector w_1 and v_1 to make $w_1^T E_0^T F_0 x_1$ maximum. Equation 4 can be solved by calculating the eigenvalue and eigenvector of matrix $M = E_0^T F_0 F_0^T E_0$. The eigenvector corresponding to largest eigenvalue θ_1^2 was the solution w_1. Then, v_1 can be computed from Equation 5:

$$v_1 = \frac{1}{\theta} F_0^T E_0 w_1 \tag{5}$$

Step 2: To build linear regressions of E_0 and F_0 from t_1, as shown in following:

$$\begin{cases} E_0 = \hat{t}_1 \alpha_1^T + E_1 \\ F_0 = \hat{t}_1 \beta_1^T + F_1 \end{cases} \tag{6}$$

where, E_1 and F_1 are the residual matrix. α_1 and $\beta_1$are vector of coefficients, can be calculated by least square methods as shown in following:

$$\begin{cases} \alpha_1 = E_0^T \hat{t}_1 / \|\hat{t}_1\|^2 \\ \beta_1 = F_0^T \hat{t}_1 / \|\hat{t}_1\|^2 \end{cases} \tag{7}$$

Step3: Then, iteration method was employed with the residual matrix E_1 and F_1 in the same manner. The results of second components were shown in Equation 8, 9, and 10, as following:

$$\hat{t}_2 = E_1 w_2, \hat{u}_2 = F_1 v_2 \tag{8}$$

$$\begin{cases} \alpha_2 = E_1^T \hat{t}_2 / \|\hat{t}_2\|^2 \\ \beta_2 = F_1^T \hat{t}_2 / \|\hat{t}_2\|^2 \end{cases} \tag{9}$$

$$\begin{cases} E_0 = \hat{t}_1 \alpha_1^T + \hat{t}_2 \alpha_2^T + E_2 \\ F_0 = \hat{u}_1 \beta_1^T + \hat{u}_2 \beta_2^T + F_2 \end{cases} \tag{10}$$

Step 4: if r is the rank of E_0, or rth components were iterated in regression, and residual matrix E_r and F_r are small enough, as shown in Equation 11, the iteration will stop.

$$\begin{cases} E_0 = \hat{t}_1 \alpha_1^T + \cdots + \hat{t}_r \alpha_r^T + E_r \\ F_0 = \hat{u}_1 \beta_1^T + \cdots + \hat{u}_r \beta_r^T + F_r \end{cases} \tag{11}$$

The final regression model Equation 13 can be calculated form Equation 12.

$$Y = t_1 \beta_1 + \cdots + t_r \beta_r \tag{12}$$

$$y_q = w_{q1} x_1 + \cdots + w_{qn} x_n \ (q = 1, 2, \ldots, m) \tag{13}$$

2.2.2 Sparse linear regression

Sparse linear regression method (SLiR) was developed (Sato et al., 2001) and became an open source toolbox, which wildly used in neural research, including reconstructing finger-movements, finger force, and arm EMG patterns from neural firings (Ting et al., 2008), blood oxygen level-dependent signals (Ganesh et al., 2008), near-infrared spectroscopy signals (Nambu et al., 2009), cortical current dipoles (Toda et al., 2011), EEG signals (Yoshimura et al., 2012), and local field potential (LFP) signals (Watanabe et al., 2012). The SLiR algorithm calculates the linear weight and automatic relevance determination (ARD) parameters in prediction model (Neal et al., 1998), which represent how the elements contribute to prediction model.

Then, SLiR sets a part of the linear weight value to zero, according with the weight contributes to the reconstruction to select the effective channels for better prediction.

Chapter 3

Prediction of hand trajectory from ECoG signals

3.1 Introduction

Over the past two decades, brain-machine interfaces (BMI) have been developed utilizing the growing understanding of brain function and the development of technology to measure brain activity. BMIs translate brain signals into commands for controlling devices such as cursors (Wolpaw et al., 1991), spelling devices (Birbaumer et al., 1999), robot arms, and neural prosthetics (Chapin et al., 1999, Wessberg et al., 2000, Taylor et al., 2002, and Carmena et al., 2003). This new communication pathway has not only the potential to help to disabled persons but also provide insight into the motor system of the brain (Wolpaw et al., 2004, Lebedev et al., 2005, Hochberg et al., 2006, Fagg et al., 2007, Velliste et al., 2008, Hochberg et al., 2012, and Hauschild et al., 2012). A number of methods have been developed to measure brain signals. BMIs are mainly categorized into two types, invasive and non-invasive BMIs, according to the signal source. BMI systems have been developed using modalities such as multi-neuron activity (Sanchez et al., 2004, and Tankus et al., 2012), local field potentials (Rickert et al., 2005, and Kellis et al., 2010), electroencephalography (Wolpaw et al., 1991, Wolpaw et al., 2004, Thulasidas et al., 2006, and Hadjidimitriou et al., 2012), and functional magnetic resonance imaging (Shibata et al., 2011).

Electrocorticography (ECoG) has been in focus as a less invasive recording method for BMIs (Leuthardt et al., 2004, Wilson et al., 2006, Chin et al., 2007, Chao et al., 2010, Shimoda et al., 2012, Pistohl et al., 2012, and Wang et al., 2013) since the first ECoG-based BMI succeeded in one-dimensional cursor control in human subjects (Leuthardt et al., 2004). ECoG signals have higher signal-to-noise ratio and spatiotemporal resolution than non-invasive recording methods, because ECoG electrodes are laid on the surface of the cerebral cortex. ECoG recording has also been shown to have long-term stability (Chao et al., 2010, and Shimoda et al., 2012), and its level of clinical risk is lower compared with invasive methods, because the electrodes do not penetrate the brain. Classifications of arm movement direction (Wilson et al., 2006, and Chin et al., 2007), 3D cursor control (Wang et al., 2013), natural grasp type (Pistohl et al., 2012 and Pistohl et al., 2013), and hand posture (Yanagisawa et al., 2012 and Chestek et al., 2013) have been achieved by using ECoG signals. Two-dimensional (Schalk et al., 2007 and Pistohl et al., 2008) and three-dimensional (3D) hand trajectories (Chao et al., 2010, and Shimoda et al., 2012) and muscle activities (Shin et al., 2012) have been decoded using epidural or subdural ECoG signals in time series. Despite these successes, however, which locations are most effective for ECoG-based hand trajectory prediction and how different numbers of effective ECoG signals affect decoding performance are still open questions.

In this study, and in investigation of these questions, we attempted to decode hand trajectory from ECoG signals. We recorded 15 and 32 ECoG signals of the primary motor cortex (Ml) and 3D hand positioning simultaneously in two

Japanese monkeys while they performed reaching and grasping tasks. We predicted 3D hand trajectories using our previous signal preprocessing method (Shin et al., 2012) and a partial least squares (PLS) method. Two methods for electrode selection were proposed in order to examine the questions previously mentioned. Prediction performances with different combination of electrodes using the proposed decoding methods were compared. Both methods showed equivalent ability to predict hand trajectories. Our results indicated that 3D hand trajectories can be predicted using nine or ten ECoG signals and that ECoG electrodes with higher performance were concentrated at the lateral areas and areas close to the central sulcus (CS).

3.2 Methods

3.2.1 Ethics statement

All experimental procedures were performed in accordance with the Guidelines for Proper Conduct of Animal Experiments of the Science Council of Japan and approved by the Committee for Animal Experiments at the National Institutes of Natural Sciences (Approval No.: 11A157). The animals' welfare and steps taken to ameliorate suffering were in accordance with the recommendations of the Weatherall report, "The use of non-human primates in research". The animals were monitored closely, and their welfare was assessed on a daily basis, or several times a day if necessary. This included veterinary examinations to ensure that they were not suffering, as well as the use of analgesics, antiemetics, or antibiotic therapy if necessary. The animals were housed individually on a 12-hour light/dark cycle and provided a rubber toy and ample food and water in their home cage. No animals were sacrificed in this study.

3.2.2 Behavioral Task

Two Japanese macaques (Monkey A: male, 8.9 kg; Monkey B: female, 4.7 kg) were trained to perform right hand reaching, grasping, pulling, and releasing tasks as shown in Figure 3-1A. The monkeys performed these tasks repeatedly and continuously for over 700 s. Monkey A performed a total of 134 trials, and monkey B performed 248 trials.

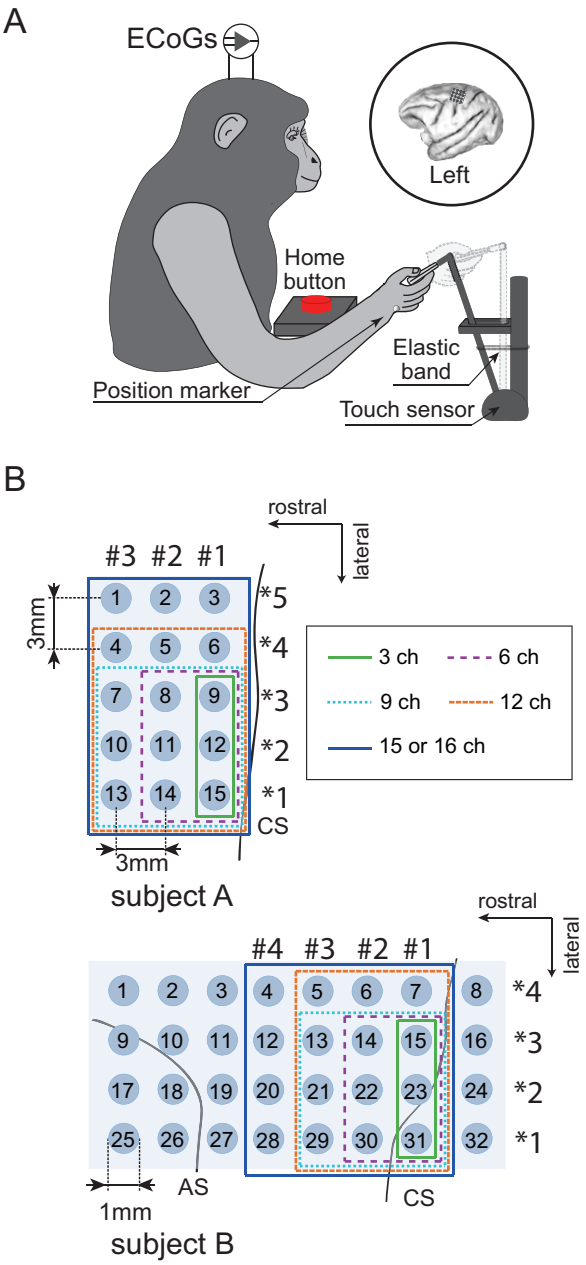

Figure 3-1. Behavioral task and location of ECoG electrodes used in decoding

A) Monkeys performed right hand reaching, grasping, pulling, and releasing tasks in a 3D workspace. During the task, ECoG and hand positioning were recorded simultaneously.

B) The planar-surface platinum electrode arrays were implanted on the gyrus between the central sulcus (CS) and the arcuate sulcus (AS) in the primary motor area in left hemisphere. The locations of all 15 and 32 electrodes in monkey A and monkey B are shown with defined channel numbers.

Locations of 3, 6, 9, 12, and 15 or 16 electrode groups used in decoding are denoted with green solid, purple dotted, blue dotted, brown dotted, and blue solid lines, respectively. The column nearest the CS was column #1 in the rostral-caudal direction, and the row in the medial-lateral direction was row *1. Note that electrodes inside the blue line were used in both column and row decoding.

Both monkeys underwent surgery to implant an ECoG electrode array under anesthesia after they completed behavioral training. We chronically implanted a platinum ECoG array (Unique Medical Corporation, Tokyo, Japan) over the left M1, which contained 15 (monkey A: 5×3 grid) and 32 (monkey B: 4×8 grid) channel electrodes, as shown in Figure 3-1B. For both monkeys A and B, centers of electrodes in column #1 (monkey A： 3, 6, 9, 12, 15; monkey B: 7, 15, 23, 31) were placed 1-2 mm rostral of the central sulcus. Electrode 31 in monkey B was placed 1-2 mm caudal of the central sulcus. Descriptions of the technical and surgical details can be found in our previous work (Shin et al., 2012).

Data recording

ECoG signals were sampled at 4 kHz using an acquisition processor system (Plexon MAP System; Plexon, Inc., Dallas, US). ECoG signals were filtered with band-pass filters through multi-channel bio-signal amplifiers (monkey A: 1.5 Hz high-pass and 1 kHz low-pass analog filters, MEG-6116, Nihon Kohden Corporation, Tokyo, Japan; monkey B: 0.7 Hz high-pass and 8 kHz low-pass analog filters, Plexon, Inc., Dallas, USA).

3D-positions of various points of the right arm were recorded using reflective markers tracked with an optical motion capture system (Eagle Digital System; Motion Analysis Corporation, Santa Rosa, CA). The system used twelve infrared

cameras operating at 200 frames/s to track the positions of multiple reflective markers (4-mm-diameter spheroids). A total of fourteen markers were attached to the right arm of each monkey but we used only the wrist marker to extract hand positioning. In addition to optical data, the motion capture system also recorded analog signals from the external stimulator (SEN-8203; Nihon Kohden Corporation, Tokyo, Japan) for synchronization with the neural recordings. The neural data were down-sampled to 500 samples per second, and the motion data were up-sampled to 500 samples per second to match the neural data, similar in manner to our previous work (Watanabe et al., 2012).

3.2.3 Preprocessing and feature selection

Raw ECoG signals were re-referenced to a common average reference (CAR) to increase the signal-to-noise ratio in the preprocessing phase. The CAR method calculates the mean of all channels, and subtracts this value from the selected output channels (McFarland et al., 1997, and Ludwig et al., 2009).

Nine specific frequency bands were selected for further analysis: δ (1.5 ~ 4 Hz), θ (4 ~ 8 Hz), α (8 ~ 14 Hz), β1 (14 ~ 20 Hz), β2 (20 ~ 30 Hz), γ1 (30 ~ 50 Hz), γ2 (50 ~ 90 Hz), γ3 (90 ~ 120 Hz), and γ4 (120 ~ 150 Hz). These specific bands were selected due to their correlation with motor activity, as shown in previous ECoG-based BMI (Schalk et al., 2007, Pistohl et al., 2008, Yanagisawa et al., 2012, Shin et al., 2012, Pistohl et al., 2012, Pistohl et al., 2013, and Chestek et al., 2013). Band-pass filters for each of the nine frequency bands were used to transform the re-referenced ECoG signals into nine separate time series. Then, each time series

was rectified and smoothed with a Gaussian filter of 0.1 s width (σ: 0.04 s). Finally, the smoothed time series $x_{ij}(t)$ at time t were z-score normalized to produce the final ECoG source signal $z_{ij}(t)$ as follows:

$$z_{ij}(t) = \frac{x_{ij}(t) - \mu_{ij}}{\sigma_{ij}} \tag{3.1}$$

where, i and j are the electrode channel and the frequency band, respectively. μ_{ij} and σ_{ij} denote the mean value and the standard deviation of $x_{ij}(t)$ over a 2 s interval before time t, respectively. These $z_{ij}(t)$ became the final ECoG feature signals for use in hand trajectory prediction. An example ECoG feature signal during a trial movement is shown in Figure 3-2.

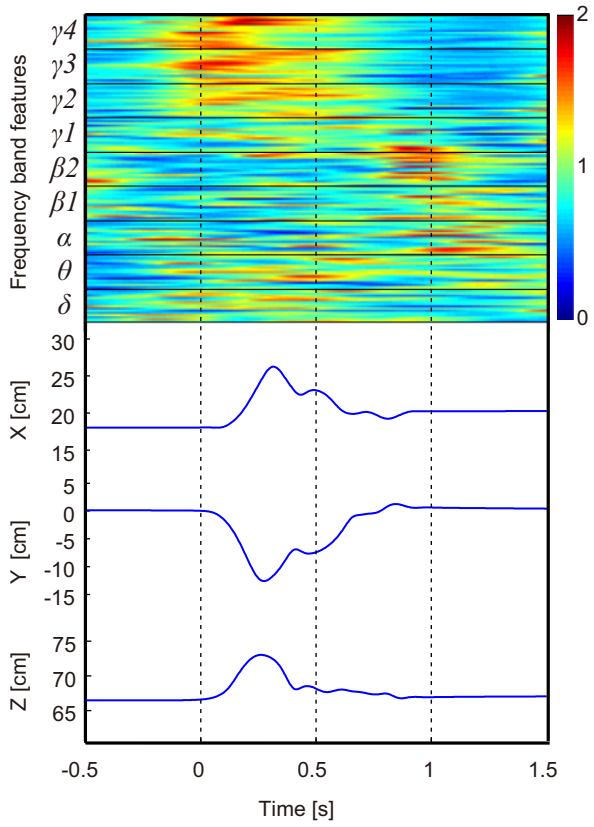

Figure 3-2. Example of measured trajectory and frequency band feature data during a movement task

Frequency band feature data were sorted into channels and frequency bands, as shown at the top. The X, Y, and Z positioning data recorded from the markers attached to the hand of monkey B, are shown at the bottom.

3.2.4 Partial Least Squares Regression

Partial least squares regression (PLS) was used to decode the 3D hand positioning from ECoG. Because of its utility in variable selection and dimension reduction, PLS has been widely used in the fields of brain imaging, computational chemistry, data mining, and others (Wold et al., 1984, Geladi et al., 1986, Rosipal et al., 2006, Chao et al., 2010, Krishnan et al., 2011, and Shimoda et al., 2012).

The 3D hand positioning at time *t*, $Y_p(t)$, was decoded using the ECoG feature signal $z_{ij}(t)$ over a 0.6 s interval before time *t* and can be described as:

$$Y_p(t) = \sum_{i=1}^{15 or 16} \sum_{j=1}^{9} \sum_{k=0}^{19} \omega_{ijk} z_{ij}(t - k\Delta t) + \omega_0 \tag{3.2}$$

where, p represents the predicted value of each xyz-coordinate, Δt is 30 ms, ω_{ijk} are the weights according to the ECoG feature signal $z_{ij}(t)$ at electrode channel i, frequency band j, and time $t - k\Delta t$, and ω_0 is the bias.

The PLS methods calculates a set of orthogonal factors called latent variables to model the relationship between two sets of data. Ten-fold cross validation was used to evaluate prediction by the model. To avoid over-fitting, the predictive error sum of squares (*PRESS*) was calculated to find the optimal number of latent variables in the PLS model, which can be described as

$$PRESS = \left\| Y_p - Y_o \right\|^2 \tag{3.3}$$

where Y_p is the predicted hand position, and Y_o is the observed hand position.

3.2.5 Two methods for electrode selection

To investigate which electrode locations were more effective, we decreased the number of electrodes for prediction using two methods and compared their respective performance.

In the first method, electrodes were selected based on their implantation position. Previous physiological studies have shown that cortico-motoneuronal cells that encode muscle-activation patterns reflected in EMG activity are located

predominantly in the anterior bank of the central sulcus (CS) (Griffin et al., 2008, and Rathelot et al., 2009). Our previous work (Shin et al., 2012) also showed that the area close to the CS might be key to decoding muscle activity. Therefore, we selected electrodes in groups of 3, 6, 9, 12, and 15 or 16 electrodes, expanding in distance from the CS as shown in Figure 3-1B. We refer to this method hereafter as location-based selection.

For the second selection method, electrodes were chosen based on prediction performance. Performance values for the PLS model using only one electrode were calculated and sorted by their coefficients of determination (R^2). Then, electrodes with high performance were added in turn to train a new PLS model. To investigate the effective frequency band for prediction, performance values for the PLS model using only δ (1.5 ~ 4 Hz), γ3 (90 ~ 120 Hz), and γ4 (120 ~ 150 Hz) bands were also calculated for each electrode. We refer to this method hereafter as performance-based selection.

3.2.6 Analysis

The entire 700 s of experiment data were divided into two parts, 500 s of training data and 200 s of test data. Ten-fold cross validation was employed to train the PLS model on the 500 s of training data. Then, the 200 s of test data were used to evaluate the PLS model.

PRESS values were calculated to find the optimal number of latent variables in the PLS model. Smaller PRESS values were associated with greater PLS model performance. Typically, the PRESS value decreases when effective latent variables

are added to train the model. Then, if over-fitting occurs, the PRESS value increases. A good choice is to stop adding latent variables as soon as the PRESS value increases. In this study, however, the PRESS value decreased quickly when the number of latent variables was within 20, but then plateaued soon after, as shown in Figure 3-4 for monkey B (see also Figure 3-3 for monkey A). Thus, we selected 20 as the optimal number of latent variable.

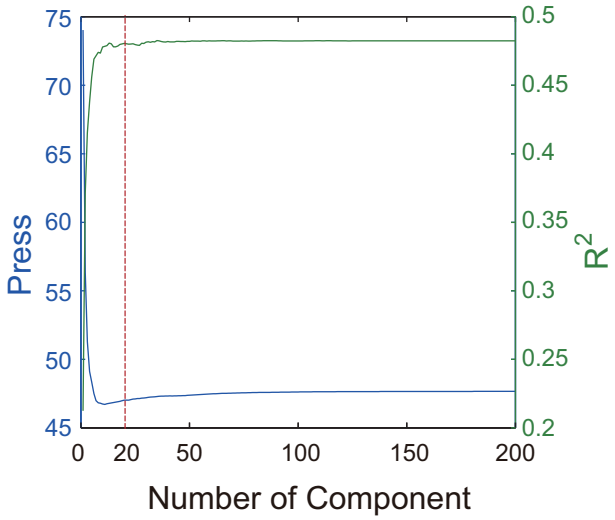

Figure 3-3. Predictive error sum of squares in model training for monkey A

The blue line and green line show predictive error sum of squares (PRESS) and R2 values, respectively, for different numbers of latent variables used in the PLS model. The optimal number of 20 is denoted with the red dotted line.

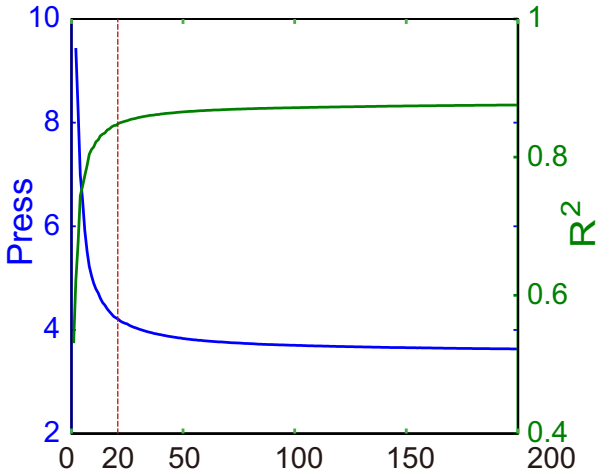

Figure 3-4. Predictive error sum of squares in model training for monkey B

The blue line and green line show predictive error sum of squares (PRESS) and R2 values, respectively, for different numbers of latent variables used in the PLS model. The optimal number of 20 is denoted with the red dotted line.

Weights of the prediction model were analyzed to evaluate the contribution of each the nine frequency bands used in this study. The contribution of frequency band Con_{fb} was calculated as

$$Con_{fb}(j) = \sum_i \sum_k |\omega_{ijk}| \Big/ \sum_i \sum_j \sum_k |\omega_{ijk}| \tag{3.4}$$

where, ω_{ijk} are the weights associated with the ECoG feature signal $z_{ij}(t)$ at electrode i, frequency band j, and time $t - k\Delta t$.

In addition, 3D hand trajectories were predicted using each of the nine frequency bands of the ECoG feature signals to investigate their individual contributions to prediction.

3.3 Result

3.3.1 Prediction with the location-based selection method

3D hand trajectories were first decoded using all the ECoG electrodes. For monkey A, the mean R^2 value and standard deviation (STD) after 10-fold cross validation were 0.4840±0.0118, and mean R^2 using the test data was 0.4806. For monkey B, the mean R^2 values after 10-fold cross validation and using the test data were 0.8424±0.0032 (Mean ± STD) and 0.7328, respectively.

We verified how decoding performance changes depending on the number of effective ECoG signals. Positions for the groups of 3, 6, 9, 12, and 15 or 16 ECoG electrodes selected to decode hand trajectories are shown in Figure 3-1B. For monkey A, R^2 values for X, Y, and Z positioning were 0.4724, 0.4695, and 0.4997, respectively, obtained using all 15 electrodes. For monkey B with all 32 electrodes, R^2 values for X, Y, and Z positioning were 0.7126, 0.7644 and 0.7263, respectively. One example of continuous prediction is shown in Figure 3-5 (see also Figure 3-7 for monkey A). Actual and predicted hand trajectories in 3D space for a single trial are also shown in Figure 3-6 (see also Figure 3-8 for monkey A). The best R^2 values for X, Y, and Z positioning were 0.7288, 0.7677, and 0.7526, respectively, obtained using 9 electrodes of monkey B.

Figure 3-9 shows prediction results over 8 s of test data using 3, 6, 9, 12, and 16 ECoG electrodes for monkey B (see also Figure 3-10 for monkey A). With the location-based selection method, 67.3% and 92.9% of the best R^2 values were

achieved with 3 electrodes for monkeys A and B, respectively. Best R^2 percentages using 6 electrodes were 85.3% and 96.9%, and 97.9% and 100% using 9 electrodes.

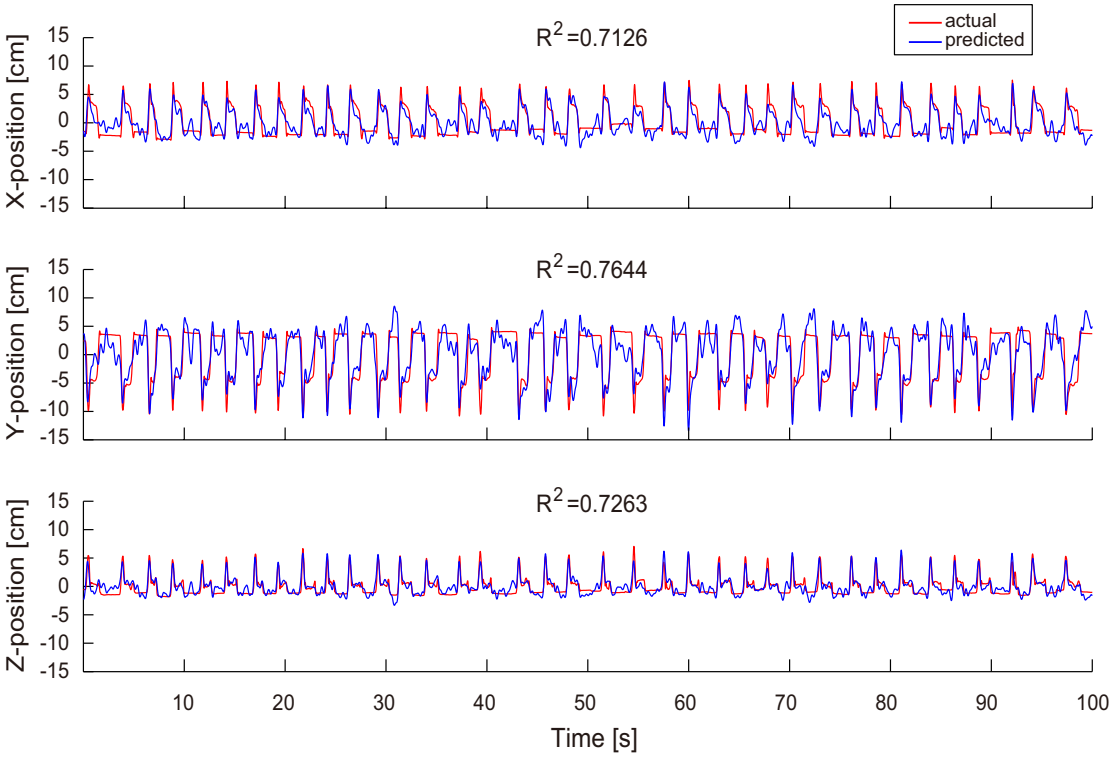

Figure 3-5. Decoding results using 32 electrodes selected with the location-based method for monkey B

Example of 3D hand trajectory prediction over 100 s of test data using 32 channel ECoG signals. R2 values between the predicted (blue) and observed (red) trajectories for X-, Y-, and Z-positions are shown.

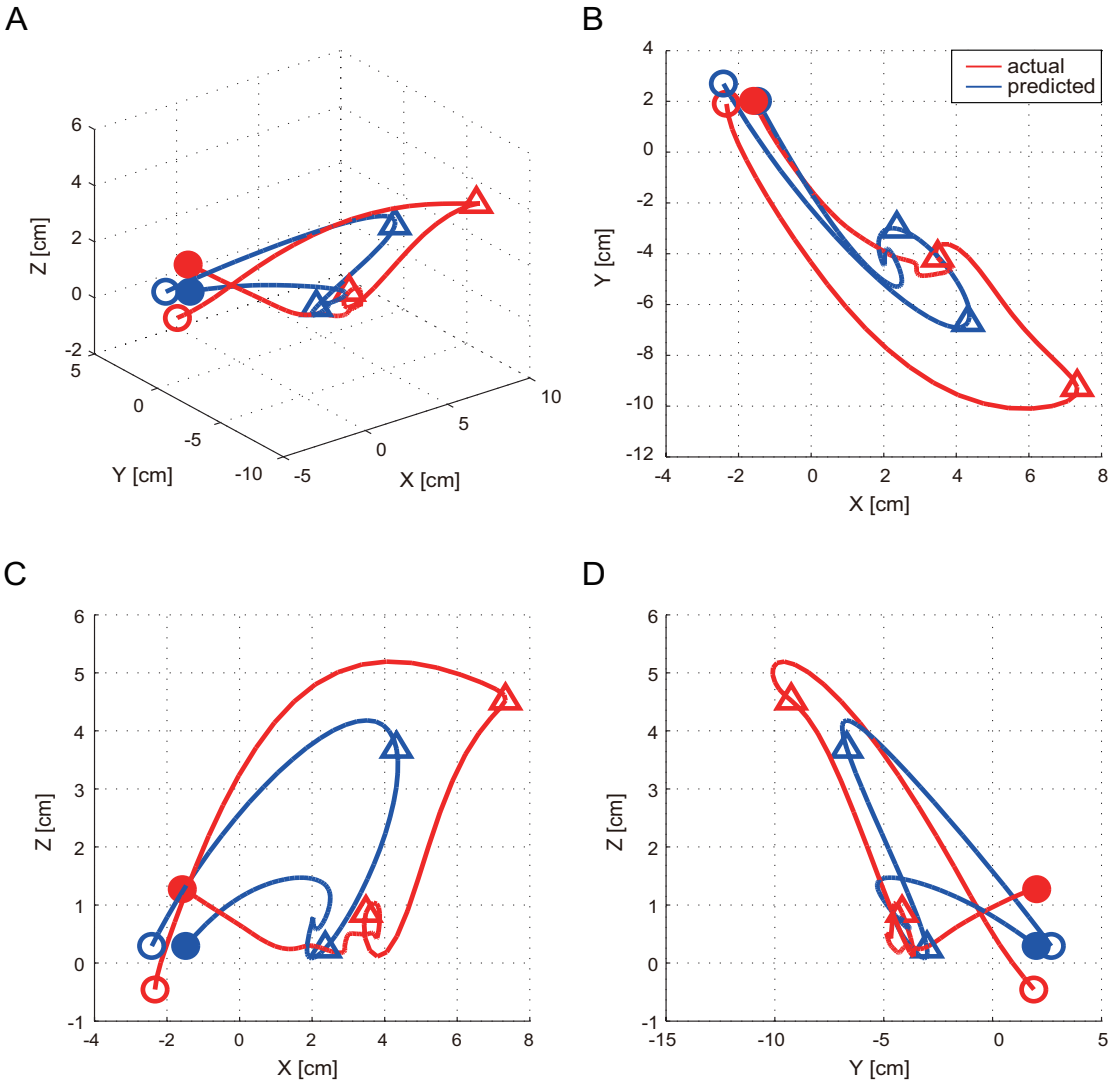

Figure 3-6. Decoding result of monkey B in three dimensional space

A) Example of prediction of 3D hand positions during 1 trial movement by using 32 channel ECoG signals. The predicted (blue) and observed (red) trajectories in 3D space are shown. The hollow circle showed the start point of movement. Two triangles showed hand position in moving process at the same time. Solid circle showed the end point of movement.

B) The predicted (blue) and observed (red) trajectories were shown in the view point of X-Y plane.

C) The predicted (blue) and observed (red) trajectories were shown in the view point of X-Z plane.

D) The predicted (blue) and observed (red) trajectories were shown in the view point of Y-Z plane.

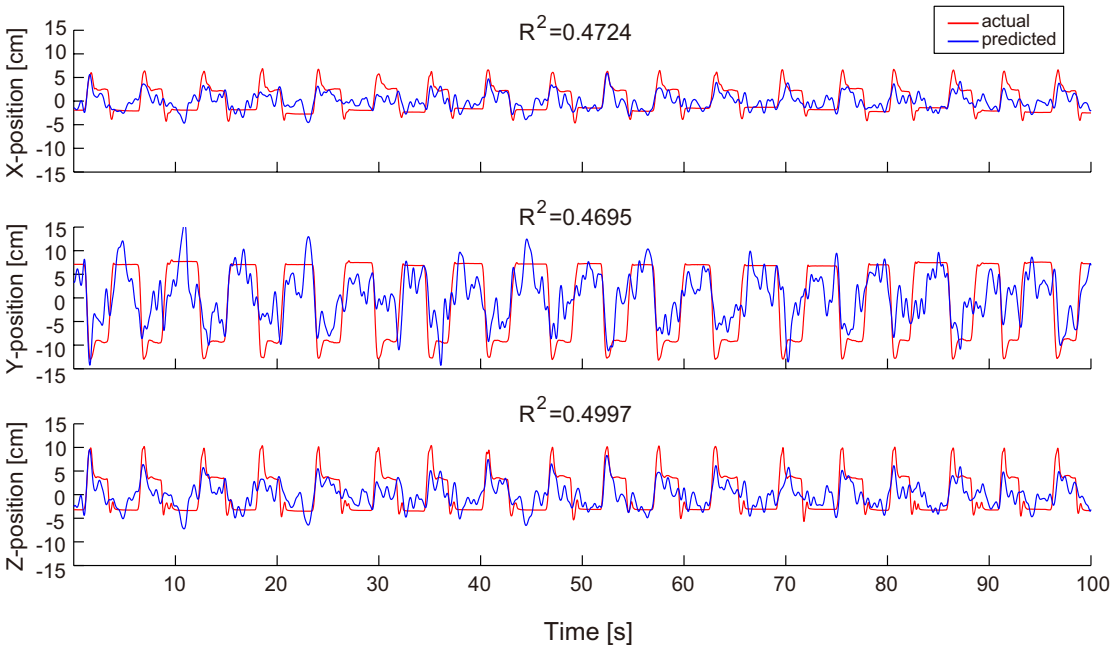

Figure 3-7. Decoding results using 15 electrodes for monkey A

Example of prediction of 3D hand positions during 100 seconds test data by using 15 channel ECoG signals. The R2 value between the predicted (blue) and observed (red) trajectories for X-, Y-, and Z-positions are shown.

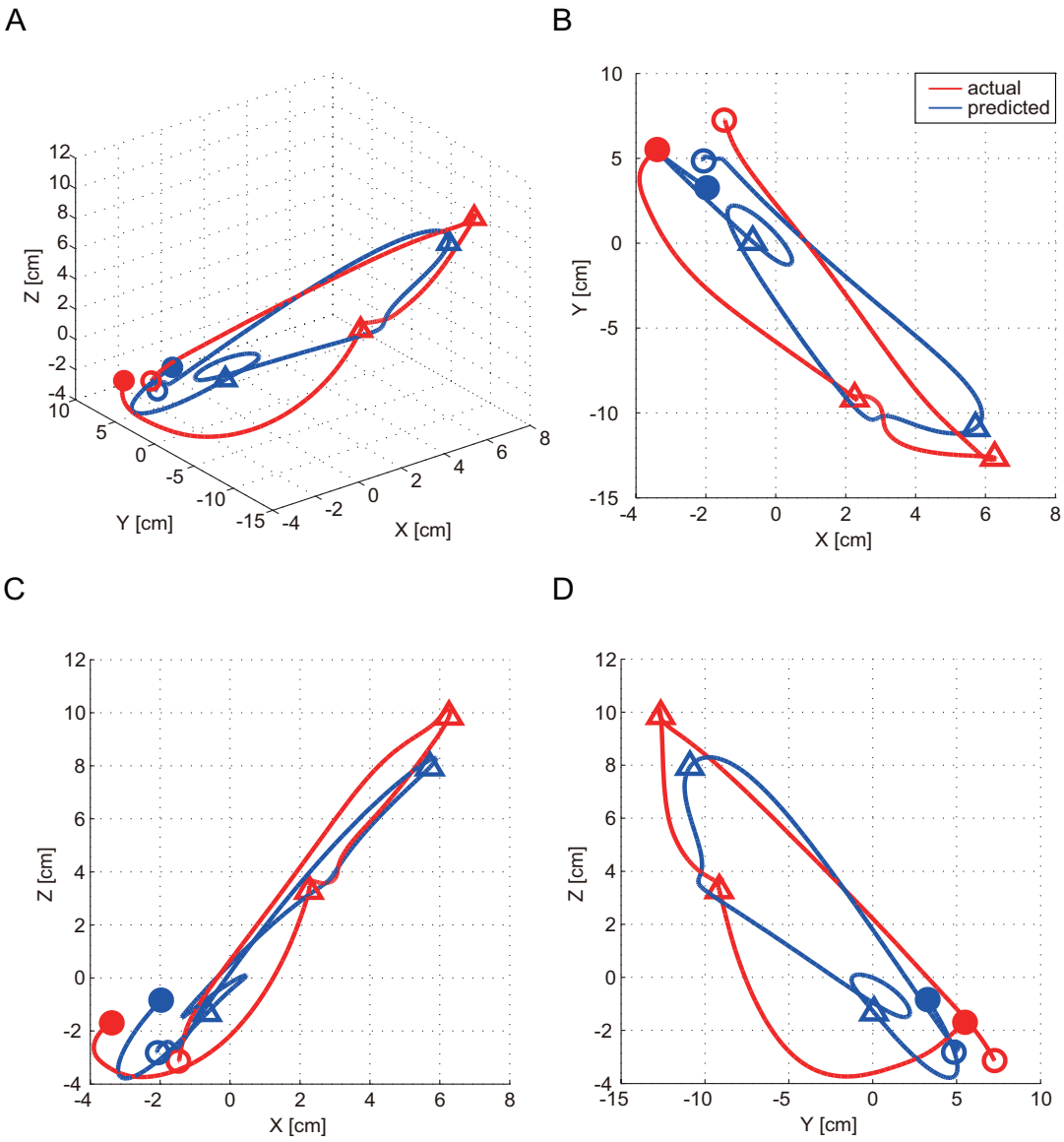

Figure 3-8. Decoding results for monkey A in three dimensional space

A) Example of 3D hand trajectory prediction for one trial movement using 3 electrodes. The predicted and observed trajectories in 3D space are depicted in blue and red, respectively. The unfilled circles represent the start point of movement. The two triangles mark hand position at equivalent time points during movement. Solid circles denote the end point of movement.

B, C, and D) The predicted (blue) and observed (red) trajectories shown in the X-Y, X-Z, and Y-Z planes, respectively.

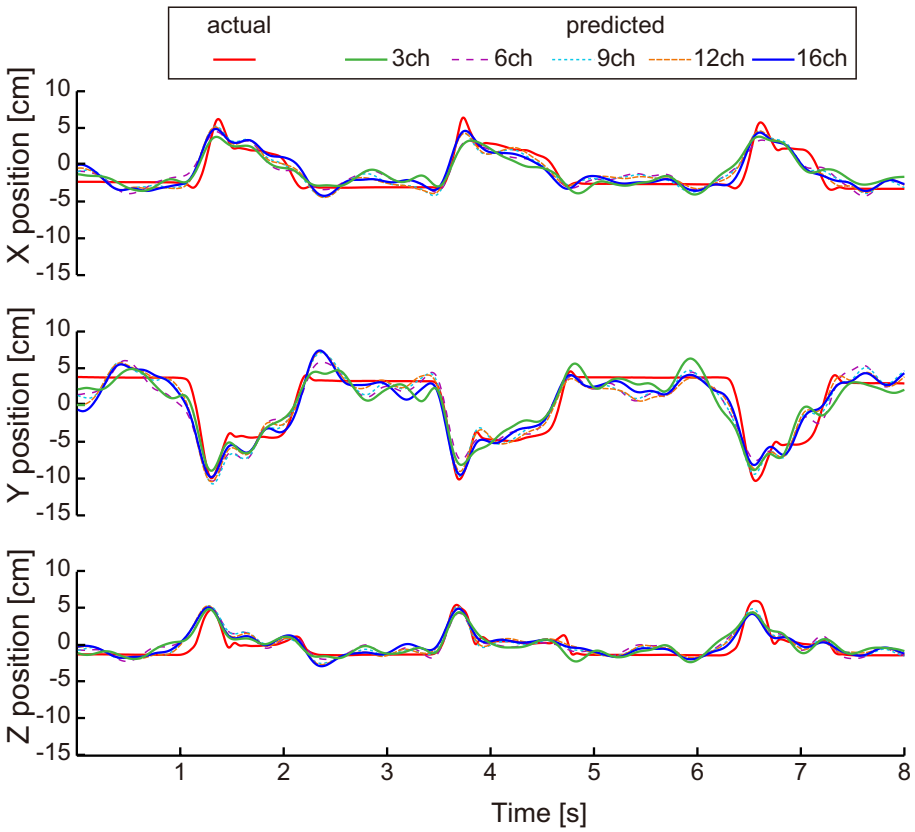

Figure 3-9. Decoding results for monkey B with different electrode numbers selected using the location-based method

Example prediction of 3D hand positioning over 8 s of test data using 3, 6, 9, 12, and 16 electrodes. The red solid line depicts actual trajectories. The green solid line, purple dotted line, light blue dotted line, brown dotted line, and blue solid line represent predicted trajectories using 3, 6, 9, 12, and 16 electrodes, respectively.

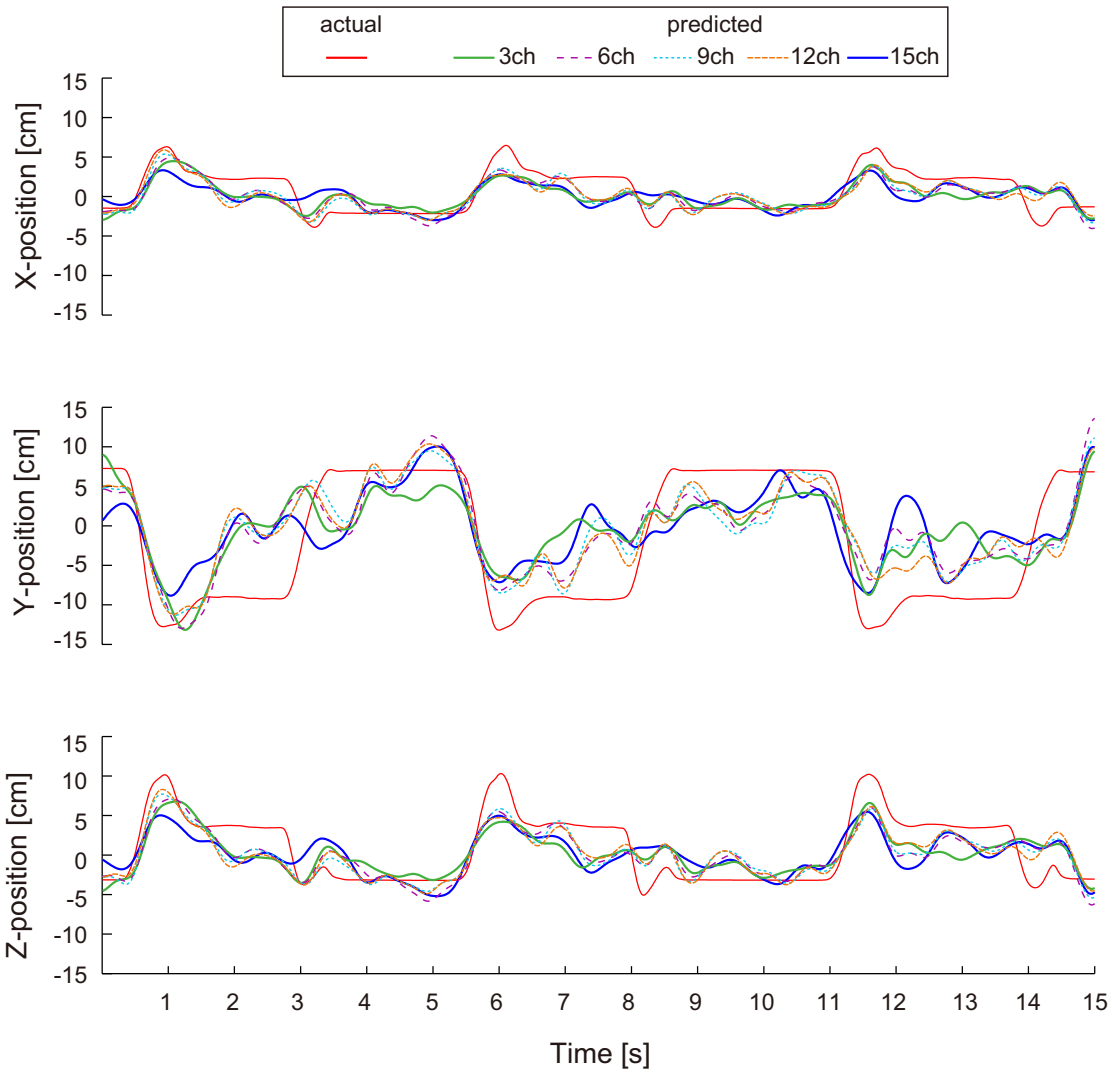

Figure 3-10. Decoding results for monkey A with different electrode numbers selected using the location-based method

Example prediction of 3D hand positioning over 8 s of test data using 3, 6, 9, 12, and 15 electrodes. The red solid line depicts actual trajectories. The green solid line, purple dotted line, light blue dotted line, brown dotted line, and blue solid line represent predicted trajectories using 3, 6, 9, 12, and 15 electrodes, respectively.

3.3.2 Prediction with the performance-based selection method

For the performance-based method, prediction results for each individual electrode are shown in Figure 3-11A. For monkey A, R^2 values ranged from 0.0903 to 0.2407. The highest R^2 value was achieved with electrode 10. For monkey B, R^2 values ranged from 0.3566 to 0.6269. The highest R^2 value was achieved with electrode 23. Prediction results for each electrode using δ (1.5 ~ 4 Hz), γ3 (90 ~ 120 Hz), and γ4 (120 ~ 150 Hz) bands are shown in Figure 3-11B, 3-11C, 3-11D, respectively. R^2 values using the δ band ranged from 0.00 to 0.05 and from -0.06 to 0.37 for monkey A and monkey B, respectively. R^2 values using the γ3 band ranged from 0.01 to 0.11 and from 0.01 to 0.50, respectively. The R^2 values using γ4 ranged from 0.01 to 0.16 and from 0.01 to 0.47, respectively. Performances for the γ3 and γ4 bands were similar and generally higher than those of the δ band. For both monkeys, the most effective electrodes were concentrated at the lateral areas and areas close to the CS, especially for the γ3 and γ4 bands.

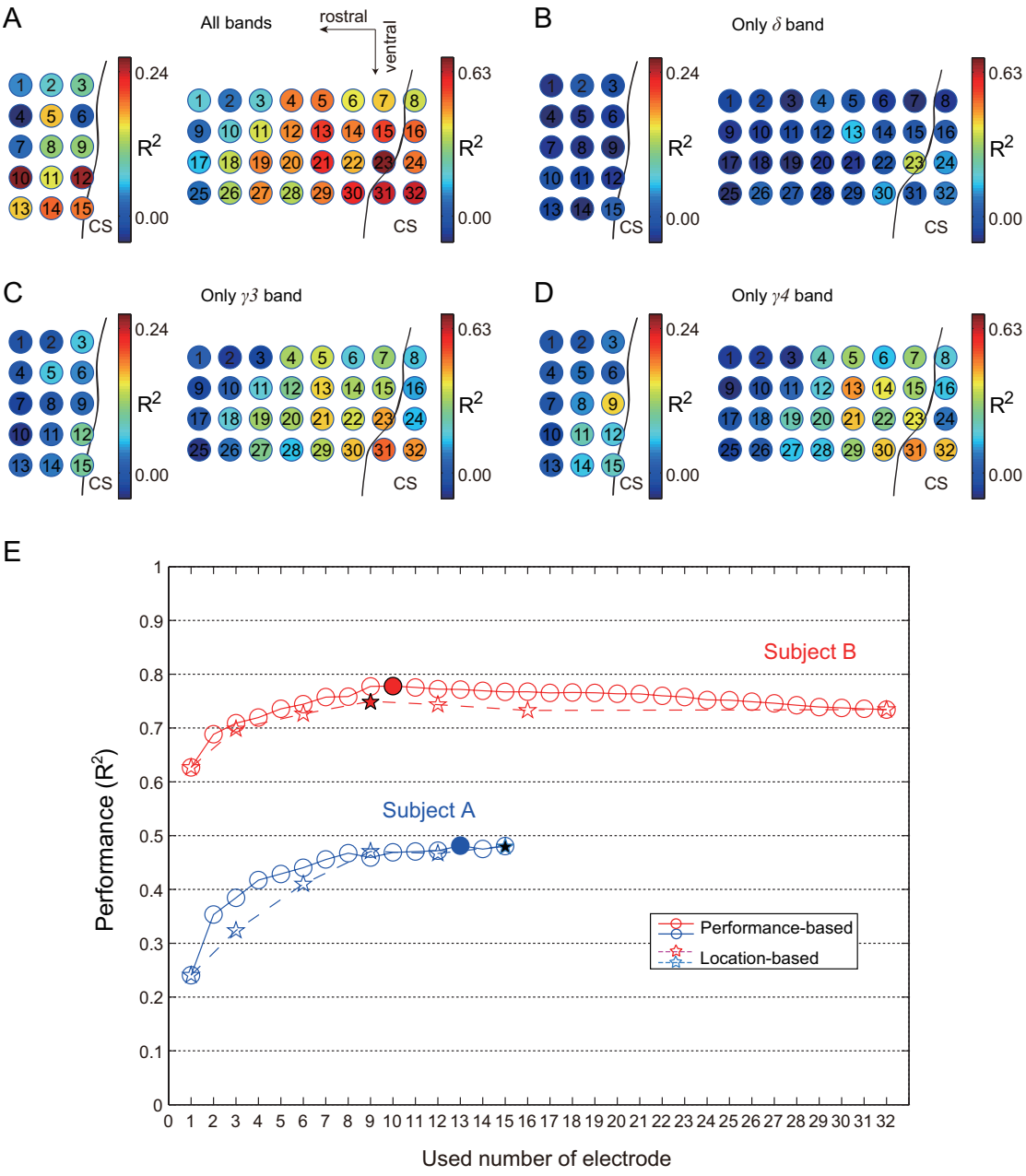

Figure 3-11. Decoding result form each electrode and performance details of two methods.

A) Performance of prediction by using all frequency bands of one electrode. The color map in each electrode showed the performance by using this electrode. For monkey A, the R^2 value changed form 0.00 to 0.24. For monkey B, the R^2 value changed form 0.00 to 0.63.

B) Performance of prediction by using δ bands of one electrode. The color map in each electrode showed the performance by using this electrode. For monkey A, the R^2 value changed form 0.00 to 0.24. For monkey B, the R^2 value changed form 0.00 to 0.63.

C) Performance of prediction by using γ3 bands of one electrode. The color map in each electrode showed the performance by using this electrode. For monkey A, the R^2 value changed form 0.00 to 0.24. For monkey B, the R^2 value changed form 0.00 to 0.63.

D) Performance of prediction by using γ4 bands of one electrode. The color map in each electrode showed the performance by using this electrode. For monkey A, the R^2 value changed form 0.00 to 0.24. For monkey B, the R^2 value changed form 0.00 to 0.63.

E) The blue solid and dotted line showed the decoding performance for Subject A by using performance-based method and location-based method, respectively. The red solid and dotted line showed the decoding performance for Subject B by using performance-based method and location-based method. The solid pentagrams and circles showed the highest performance in performance-based method and location-based method, respectively. The green and brown dotted line showed the number of electrodes, by using which to achieve 90% of best R^2 value, for monkey A and monkey B, respectively, in location-based methods.

3.3.3 Summary of the two electrode selection methods

Performance details of two electrode selection methods are shown in Figure 3-11E. For both monkeys, performance was improved quickly as the number of electrodes used increased from 1 to 9. The performance curves fluctuated only slightly when using 10 electrodes and above. The best R^2 values were achieved using 13 and 10 electrodes for monkeys A and B, respectively.

For both methods, the principle is to select more effective electrodes in prediction. As shown in Figure 3-11A, 3-11B, 3-11C, and 3-11D, higher

performance electrodes are concentrated at the lateral areas and near areas of CS. This result is consistent with the principle of the location-based selection method.

To confirm this principle, columns electrodes were also used to predicted hand trajectory. Prediction results in the rostral-caudal direction, and in the medial-lateral direction are shown in Table 1 and Table 2, respectively.

The highest performance in the rostral-caudal direction was achieved using column #1 in both monkeys. For monkey A, performance using column #3 was higher than that using #2. This might have been an effect of the presence of electrode 10 (Figure 3-11A). For monkey B, performance using column #3 was second highest, and performance using column #2 was higher than that using column #4. Highest performance in the medial-lateral direction was achieved using row *2 in both monkeys. For monkey A, performance using row *1 was higher than that using rows *3, *4, and *5. For monkey B, performance using row *3 was second highest, and may have been due to the effect of the δ band at electrode 13 (Figure 3-11B). Performance using row *1 was higher than that using row *4. Generally, higher performance rows and columns are at the lateral areas and areas near the CS.

Table 3-1. Prediction results using location-based electrode selection in the rostral-caudal direction

Monkey	Location	R^2			
		x	y	z	mean
A	#1	0.3317	0.3397	0.3535	**0.3416**
	#2	0.2959	0.2452	0.3438	0.2950
	#3	0.2998	0.2956	0.3580	0.3178
B	#1	0.6773	0.7164	0.6980	**0.6973**
	#2	0.6063	0.6593	0.6524	0.6393
	#3	0.6591	0.6793	0.6704	0.6696
	#4	0.5655	0.6059	0.5578	0.5763

Table 3-2. Prediction results using location-based electrode selection in the medial-lateral direction

Monkey	Location	R^2			
		x	y	z	mean
A	*1	0.3035	0.3008	0.3429	0.3157
	*2	0.3640	0.3774	0.4141	**0.3852**
	*3	0.2423	0.2217	0.2873	0.2505
	*4	0.1996	0.1807	0.2381	0.2061
	*5	0.1851	0.1713	0.2213	0.1926
B	*1	0.6343	0.6888	0.6117	0.6449
	*2	0.6577	0.6930	0.7069	**0.6859**
	*3	0.6646	0.7005	0.6841	0.6830
	*4	0.5729	0.5865	0.5501	0.5699

3.3.4 Analysis of specific frequency bands

Weights of the nine frequency bands in the prediction model were calculated and are shown in Figure 3-12A as percent contributions. For monkey B, γ3 (90 ~ 120 Hz) provided the highest contribution. The contributions of δ (1.5 ~ 4 Hz) and γ4 (120 ~ 150 Hz) were higher than those of θ (4 ~ 8 Hz), α (8 ~ 14 Hz), β1 (14 ~ 20 Hz), and β2 (14 ~ 20 Hz).

3D hand trajectories were predicted by using each frequency band of the ECoG feature signals individually (Table 3). A two-way ANOVA was employed to judge two effects (X, Y, and Z positioning, and the nine frequency bands). No significant differences in prediction performance between X, Y, and Z positioning were observed in both monkeys (monkey A: $F_{2, 16} = 3.61$, $p = 0.051$; monkey B: $F_{2, 16} = 1.96$, $p = 0.173$). Significant differences in prediction performance were observed between frequency bands, (monkey A: $F_{8, 16} = 14.16$, $p = 6.41\times10^{-6}$; monkey B: $F_{8, 16} = 52.39$, $p = 4.99\times10^{-10}$), as shown in Figure 3-12B. The prediction performances using δ, γ2, γ3, and γ4 bands were also significantly higher than that of other bands. Prediction performance of the θ and γ1 bands was significantly higher than that of β2.

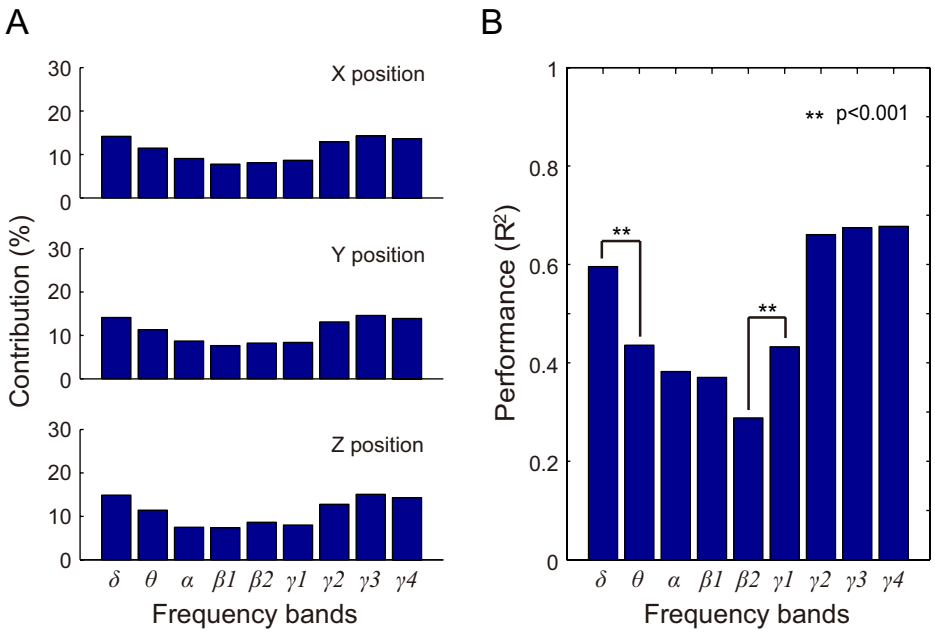

Figure 3-12. Analysis results of monkey B on separate sensorimotor rhythm bands.

A) The weight of each frequency band in PLS model was calculated and showed. Each bar represents the weights of each frequency band. Each plane showed the contribution of X position, Y position and Z position, respectively.

B) Result of prediction using each separate sensorimotor rhythm ECoG signals. The result of analysis based on two-way ANOVA (position and sensorimotor rhythm band) was shown. Each bar represents the mean of R^2 value of X, Y, Z position between observed and predicted hand trajectories. Significant differences between the mean of R^2 value are marked with * ($p<0.001$)

Table 3-3. Prediction results using individual frequency bands

Monkey	Bands	R^2			
		X	y	z	mean
A	δ	0.0987	0.0440	0.1121	0.0850
	θ	0.0689	0.0873	0.0757	0.0773
	α	0.0793	0.1094	0.0800	0.0895
	β1	0.1314	0.1206	0.1503	0.1341
	β2	0.1860	0.2108	0.2188	0.2052
	γ1	0.1627	0.1808	0.1634	0.1690
	γ2	0.1604	0.1476	0.2033	0.1705
	γ3	0.1602	0.1149	0.1920	0.1557
	γ4	0.1739	0.1584	0.2103	0.1809
B	δ	0.5652	0.5970	0.6242	0.5955
	θ	0.4316	0.4496	0.4263	0.4358
	α	0.4169	0.4252	0.3051	0.3824
	β1	0.3743	0.4049	0.3318	0.3703
	β2	0.2906	0.3389	0.2345	0.2880
	γ1	0.4567	0.4796	0.3618	0.4327
	γ2	0.6391	0.6794	0.6628	0.6605
	γ3	0.6427	0.6844	0.6966	0.6746
	γ4	0.6477	0.6913	0.6929	0.6773

3.4 Discussion

3.4.1 main work in this study

This study decoded 3D hand trajectories from ECoG signals in Ml and showed that most effective electrodes were concentrated at the lateral areas and areas close to the CS. Comparisons between prediction results suggest that a selection of effective ECoG signals may be better choice than a whole ECoG array. Our results also suggested that ECoG signals are of ample quality and efficiency to control a high performance neural prosthetic.

3.4.2 Which locations are most effective for prediction?

Carmena et al. (2003) reported that neuron activity recorded from Ml showed greater efficacy than that from dorsal premotor cortex, supplementary motor cortex, posterior parietal cortex, and primary somatosensory cortex. Previous ECoG studies have also used signals mainly from the primary motor area (Pistohl et al., 2012, Pistohl et al., 2013, and Yanagisawa et al., 2012). We chose M1 based on those previous results and evaluated the optimal locations in M1. As shown in Figure 3-11A, ECoG signals from the lateral areas and near areas of CS also showed greater efficacy in prediction, especially in the δ, γ3, and γ4 bands (Figure 3-11B, 3-11C, 3-11D).

3.4.3 How did different numbers of ECoG electrodes affect performance?

As shown in in Figure 3-11E, the best mean R^2 values for monkeys A and B were 0.4805 and 0.7496, respectively, in the location-based selection, and 0.4815

and 0.7780 in the performance-based selection. Both methods, therefore, appear to have equivalent ability to predict hand trajectories.

For both monkeys, performance improved quickly as the number of electrodes used increased from 1 to 9. The performance curves fluctuated only slightly when using 10 electrodes and above. Best decoding performance was achieved using a relatively small number of electrodes, 13 and 10 electrodes in the performance-based selection for monkey A and monkey B, respectively. The performances curves of this study are similar to the results of a previous neuron activity-based study (Sanchez et al., 2004), which selected different numbers of high sensitivity neurons in decoding kinematic variables. These results suggest that best decoding performance can be achieved from a relatively small number of effective ECoG signals. However, it should also be noted that decoding performance is not simply related to the electrode number but may more closely depend on the density of electrodes within the effective areas. Still, with the potential utility of wireless transmission technology in ECoG (Hirata et al., 2011, and Bjorninen et al., 2012), a relatively smaller number of electrodes would provide the benefit of lower power consumption, extending the usage time for wireless BMIs.

3.4.4 Which frequency bands are most effective?

To evaluate the efficacy of specific frequency bands in trajectory decoding, we compared prediction performances of the nine physiologically-based frequency bands with 10 Hz-width fractionized frequency bands from 0 to 150 Hz. The physiologically-based method produced nearly the same or better results (R^2 =

0.7328) than the fractionized frequency method ($R^2 = 0.6815$) for monkey B. These results suggest that the usage of physiological frequency bands is more effective than non-physiological fractionized frequency bands.

Weight analysis for the PLS model and the results of decoding performance using each of the nine frequency bands showed that the δ, γ2, γ3, and γ4 bands were more effective than other bands in this study. Previous ECoG studies have shown the importance of the high γ band in motor decoding and BMI control, such as the 60-80 Hz band in prediction of 3D hand trajectories in monkeys (Chao et al., 2010, and Shimoda et al., 2012), 70-110 Hz in controlling a 3D cursor in humans (Wang et al., 2013), and 56-128 Hz in grasp detection in humans (Pistohl et al., 2013). The importance of the δ band is also supported by our previous ECoG work (Shin et al., 2012), and is consistent with a previous study (Pistohl et al., 2012), which employed a low-frequency band (2-6 Hz) to classify natural grasp types.

Chapter 4

Prediction of grasp force profile from ECoG signals

4.1 Introduction

Brain machine interfaces (BMIs) hold promise as a means for disabled individuals to control external devices using neural activity. In the past two decades, invasive methods have been wildly used to control robot arms and other neural prosthetics in rats (Chapin et al., 1999 and Koralek et al., 2012), monkeys (Wessberg et al., 2000, Taylor et al., 2002, Carmena et al., 2003, Musallam et al., 2004, Velliste et al., 2008, Ganguly et al., 2011, Ethier et al., 2012, Gilja et al., 2012, Hauschild et al., 2012, and Hao et al., 2013), and humans (Hochberg et al., 2006, Hochberg et al., 2012, and Collinger et al., 2013), using neural signals such as spiking activity and local field potential. Muscle activity (Morrow and Miller, 2003, and Koike et al., 2006), reach and grasp kinematics (Zhuang et al., 2010, Bansal et al., 2011, and Bansal et al., 2012) and dexterous finger motions (Aggarwal et al., 2008) during real movement have also been decoded in monkeys. Despite these successes, however, the penetration of the brain with invasive methods has remained a serious bottleneck for practical clinical solutions in humans.

Electrocorticography (ECoG) signal presents a potential alternative for supporting high accuracy BMIs because of its comparatively lower invasiveness. ECoG has seen wide clinical use, with electrodes commonly being implanted to

localize seizure foci for the treatment of epilepsy in humans. This has also allowed for the investigation of ECoG-based BMI in humans, including studies on cursor control (Leuthardt et al., 2004, Schalk et al., 2008, and Wang et al., 2013), classification of hand movement (Chin et al., 2007, Yanagisawa et al., 2009, and Yanagisawa et al., 2011), and grasp types (Pistohl et al., 2012), detection of grasp initiation (Pistohl et al., 2013), and decoding of hand trajectories (Schalk et al., 2007, Chao et al., 2010, Shimoda et al., 2012, Nakanishi et al., 2013, and Chen et al., 2013) and finger movement (Kubanek et al., 2009 and Acharya et al., 2010). Prediction of muscle activity (Shin et al., 2012) and movement-related intracortical activity (Watanabe et al., 2012) from ECoG signals during reaching and grasping movements in monkeys have also been successful. Despite the importance of grasping force in everyday life, the prediction of grasp force profile during reaching and grasping movement has remained lacking yet.

The aim of this study was to decode grasp force profile from ECoG signals recorded from the primary sensorimotor areas. Fifteen and sixteen channel ECoG signals were recorded from the primary sensorimotor cortex in Japanese monkeys while performing reaching and grasping tasks. A sparse linear regression method was employed to decode grasp force profile. Our results demonstrate accurate decoding of grasp force profile from ECoG signals and the efficacy of high γ bands in decoding.

4.2 Method

4.2.1 Ethics statement

All experimental procedures were performed in accordance with the Guidelines for Proper Conduct of Animal Experiments by the Science Council of Japan and approved by the Committee for Animal Experiments at the National Institutes of Natural Sciences (Approval No.: 11A157). Steps were taken to ensure the animals' welfare and ameliorate suffering in accordance with the recommendations of the Weatherall report, "The use of non-human primates in research."

4.2.2 Monkey subjects and experimental procedure

Here, we describe our main experimental procedures. Details on these procedures can be found in Chapter 3. We trained two Japanese monkeys (Monkey A: male, 8.9 kg; Monkey B: female, 4.7 kg) to reach for and grasp a small plastic knob at the end of joystick with the right hand, repeatedly and continuously. Totals of 134 and 248 trials were performed by monkey A and monkey B, respectively.

4.2.3 ECoG and force data collection

A thin-film force sensor (FlexiForce; Tekscan, Inc., South Boston, MA) was attached to the surface of a knob to measure grasp force. As shown in Figure 4-1, 15 (monkey A: 5x3 grid) and 16 (monkey B: 4x4 grid, with one electrode in the somatosensory cortex) channel ECoG electrode arrays (Unique Medical Corporation, Tokyo, Japan) were implanted in the left primary sensorimotor areas, for monkeys A and B, respectively. Locations of these electrode arrays were

identified from anatomical views during surgeries and postoperative X-ray image (monkey B) or observation with craniotomy after perfusion (monkey A). The electrodes had a diameter of 1 mm and an inter-electrode distance of 3 mm center-to-center. ECoG signals and lateral grasp force were recorded simultaneously during the grasping task at 4kHz with an acquisition processor system (Plexon MAP System; Plexon, Inc., Dallas, TX) and down-sampled to 500Hz for data processing.

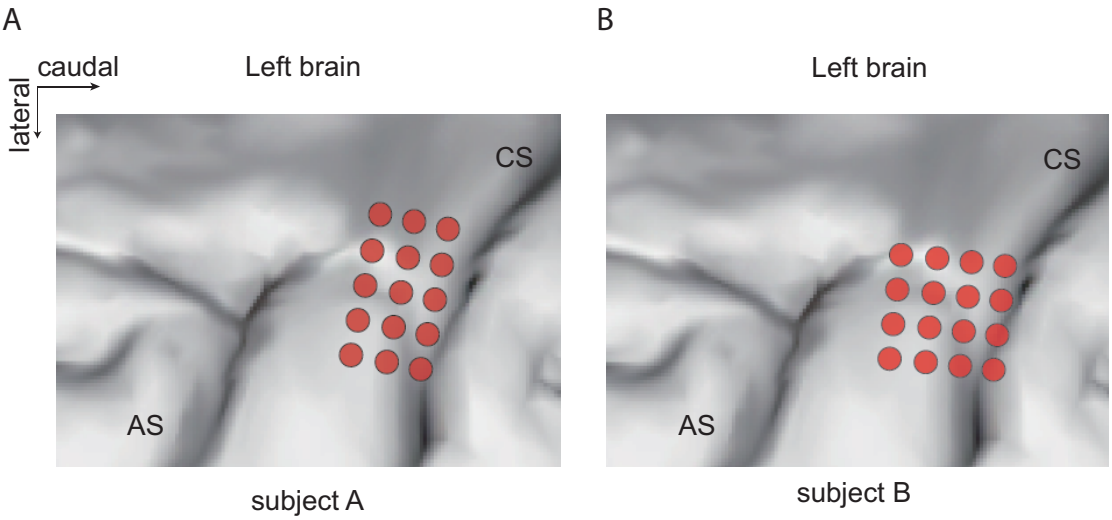

Figure 4-1. ECoG electrode locations

The ECoG platinum electrode arrays were placed on the subdural space, near the central sulcus (CS) in the left primary sensorimotor area. AS: arcuate sulcus.

4.2.4 Decoding algorithm and data analysis

We detected the start and end time points for grasping from the position of the wrist marker, a on and off target sensor information on joystick (Shin et al., 2012, and Chen et al., 2013). The start point (time point 0 in Figure 2) was defined as the time point when the monkeys touched the knob, and the end point was defined as

the time point when the monkeys released the knob. Both points were confirmed using target sensor data. Average grasping durations with standard deviations (STD) for monkeys A and B were 1.86 ± 0.21 s and 0.52 ± 0.17 s, respectively (Fig. 2). Thus, the duration of each trial was set to 2 seconds and 0.7 second in force profile prediction monkeys A and B, respectively. Ten-fold cross validation was employed to counteract over-fitting, with each fold containing 11 and 24 test trials for monkeys A and B, respectively.

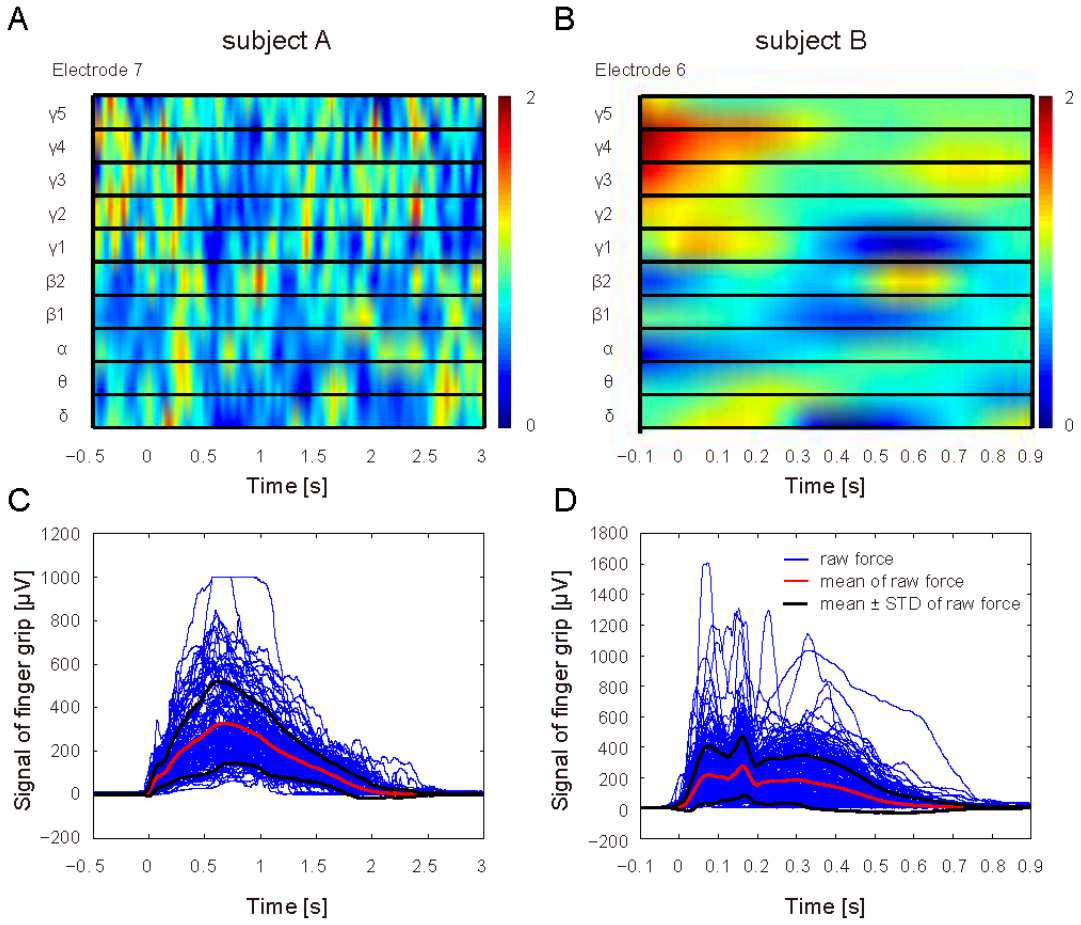

Figure 4-2. ECoG spectral feature and raw force data

A) ECoG spectral feature of the most contributed electrode 7 for monkey A

B) ECoG spectral feature of the most contributed electrode 6 for monkey B

C) Blue lines represent the amplitude of raw force for monkey A, which containing a total number of 134 trials. The red and black lines represent the mean and standard deviation of raw force, respectively.

D) Blue lines represent the amplitude of raw force for monkey B, which containing a total number of 248 trials. The red and black lines represent the mean and standard deviation of raw force, respectively.

In preprocessing, raw ECoG signals were common average referenced and band-pass filtered using ten different sensorimotor frequency band-pass filters: δ (1.5 ~ 4 Hz), θ (4 ~ 8 Hz), α (8 ~ 14 Hz), β1 (14 ~ 20 Hz), β2 (20 ~ 30 Hz), γ1 (30 ~ 50 Hz), γ2 (50 ~ 90 Hz), γ3 (90 ~ 120 Hz), γ4 (120 ~ 150 Hz), γ5 (150 ~ 200 Hz). Band-passed ECoG signals were then smoothed with a Gaussian filter (width: 0.1 s; σ: 0.04 s). Finally, the smoothed ECoG signals at time *t*, $sECoG_{ij}(t)$, were z-score normalized to produce the final ECoG source signal $z_{ij}(t)$ such that

$$z_{ij}(t) = \frac{sECoG_{ij}(t) - \mu_{ij}}{\sigma_{ij}} \tag{4.1}$$

where, *i* and *j* are the electrode channel and the frequency band, respectively, and μ_{ij} and σ_{ij} are the mean and the standard deviation of $sECoG_{ij}(t)$ over a 2 s interval before time *t*, respectively.

Force data were also low-passed filtered at a cutoff of 4Hz (100^{th} order window-based finite impulse response filter). Then, the low-passed force data were normalized to the maximum value of each trial to produce the force profile.

A sparse linear regression method was employed to train a decoding model using ECoG feature signals. Sparse estimation methods are expected to be useful for

extracting significant information from redundant and numerous dataset. We used the sparse linear regression algorithm, which has a generalization capability for unknown datasets due to its ability to remove irrelevant features, avoid over-fitting of the datasets. The grasp force profile at time *t*, $F_p(t)$, was decoded using the ECoG feature signal $z_{ij}(t)$ over a 0.6 s interval before time *t* and can be described as

$$F_p(t) = \sum_{i=1}^{15 or 16} \sum_{j=1}^{10} \sum_{k=0}^{19} \omega_{ijk} z_{ij}(t - k\Delta t) + \omega_0 \tag{4.2}$$

where, *p* is the predicted value of the grasp force profile, Δt is 30 ms, ω_{ijk} are the weights according to the ECoG feature signal $z_{ij}(t)$ at electrode channel i, frequency band j, and time $t - k\Delta t$, and ω_0 is the bias.

Weights of the prediction model were analyzed to evaluate the contribution of each electrode and frequency band used in this study. The contribution of each electrode Con_e, each frequency band Con_{fb} and the contribution matrix of electrodes and frequency bands Con_{efb} were calculated as

$$Con_e(i) = \sum_j \sum_k |\omega_{ijk}| \Big/ \sum_i \sum_j \sum_k |\omega_{ijk}| \tag{4.3}$$

$$Con_{fb}(j) = \sum_i \sum_k |\omega_{ijk}| \Big/ \sum_i \sum_j \sum_k |\omega_{ijk}| \tag{4.4}$$

$$Con_{efb}(i,j) = \sum_k |\omega_{ijk}| \Big/ \sum_i \sum_j \sum_k |\omega_{ijk}| \tag{4.5}$$

where, ω_{ijk} are the weights according to the ECoG feature signal $z_{ij}(t)$ at electrode channel i, frequency band j, and time $t - k\Delta t$.

Analysis of variance (ANOVA) was performed using MATLAB (MathWorks, Natick, MA) to detect significant effects of Con_e and Con_{fb}. A two-way ANOVA with the Tukey-Kramer test was applied to detect significant effects of Con_{efb}.

Correlation coefficient (CC) and normalized root mean square error (nRMSE) values between actual and predicted force profile were used to valuate performance of prediction.

4.3 Result

4.3.1 Decoding results of lateral grasp force profile

Grasp force profiles for monkeys A and B were predicted from the 15 and 16 channel ECoG signals, respectively. Figure 4-3 shows typical decoded and actual force profiles for both monkeys. CC and nRMSE values in 10-fold cross validation are summarized in Table 1. The best CC values for monkeys A and B were 0.82 ± 0.09 (mean ± standard deviation) and 0.79 ± 0.15, respectively. The best nRMSE values for monkeys A and B were 0.21 ± 0.05 and 0.25 ± 0.09, respectively. Grand averages and standard error of the mean were 0.77 ± 0.03 and 0.71 ± 0.05 for CC, and 0.23 ± 0.01 and 0.29 ± 0.02 for nRMSE. These results clearly show that ECoG data contained information about grasp force profile.

CC and nRMSE distributions over all test trials in 10-fold cross validation are shown in Figure 4-4. The median CC and nRMSE were 0.81 and 0.21 for monkey A, and 0.80 and 0.28 for monkey B, respectively. Negative CC values were used in analysis but not shown for ease of visualization. These results show that force profiles were predicted successfully from ECoG signals.

A one-way ANOVA was applied to identify whether significant differences exist in decoding performances between test subsets. No significant differences in CC (monkey A: $F_{9, 100} = 0.75$, $p = 0.66$; monkey B: $F_{9, 230} = 0.80$, $p = 0.62$), or nRMSE (monkey A: $F_{9, 100} = 0.34$, $p = 0.96$; monkey B: $F_{9, 230} = 0.91$, $p = 0.52$), were observed between test subsets in both monkeys.

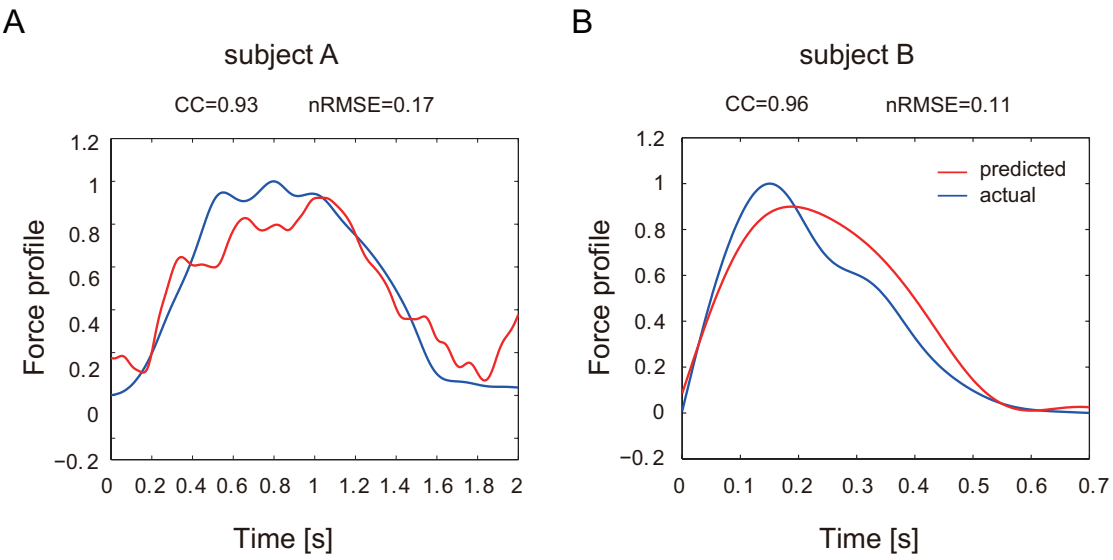

Figure 4-3. Sample of predicted force profile

A) Example of observed (blue) and predicted (red) force profile over 2 second of test data using 15 channel ECoG signals for monkey A. The coefficient of correlation (CC) value and normalized root mean square error (nRMSE) between observed and predicted force profile were showed at the top of figure. In this figure, the prediction error of the early grip strength accidentally appeared.

B) Example of observed (blue) and predicted (red) force profile over 0.7 second of test data using 16 channel ECoG signals for monkey B. The coefficient of correlation (CC) value and normalized root mean square error (nRMSE) between observed and predicted force profile were showed at the top of figure.

Table 4-1. Decoding performances of 10-fold cross validation for both monkeys

	Monkey A		Monkey B	
Test set	CC	nRMSE	CC	nRMSE
1	0.81±0.07	0.22±0.03	0.78±0.21	**0.25±0.09**
2	0.74±0.17	0.23±0.06	0.71±0.22	0.31±0.10
3	**0.82±0.09**	0.22±0.05	0.70±0.27	0.30±0.12
4	0.73±0.18	0.24±0.08	0.64±0.27	0.31±0.11
5	0.79±0.10	0.22±0.05	0.67±0.24	0.32±0.11
6	0.80±0.13	**0.21±0.05**	0.74±0.24	0.28±0.11
7	0.74±0.13	0.24±0.06	0.73±0.32	0.28±0.14
8	0.78±0.09	0.23±0.04	**0.79±0.15**	0.27±0.09
9	0.73±0.17	0.23±0.05	0.72±0.28	0.29±0.13
10	0.79±0.13	0.22±0.06	0.67±0.32	0.28±0.10
Average	0.77±0.03	0.23±0.01	0.71±0.05	0.29±0.02

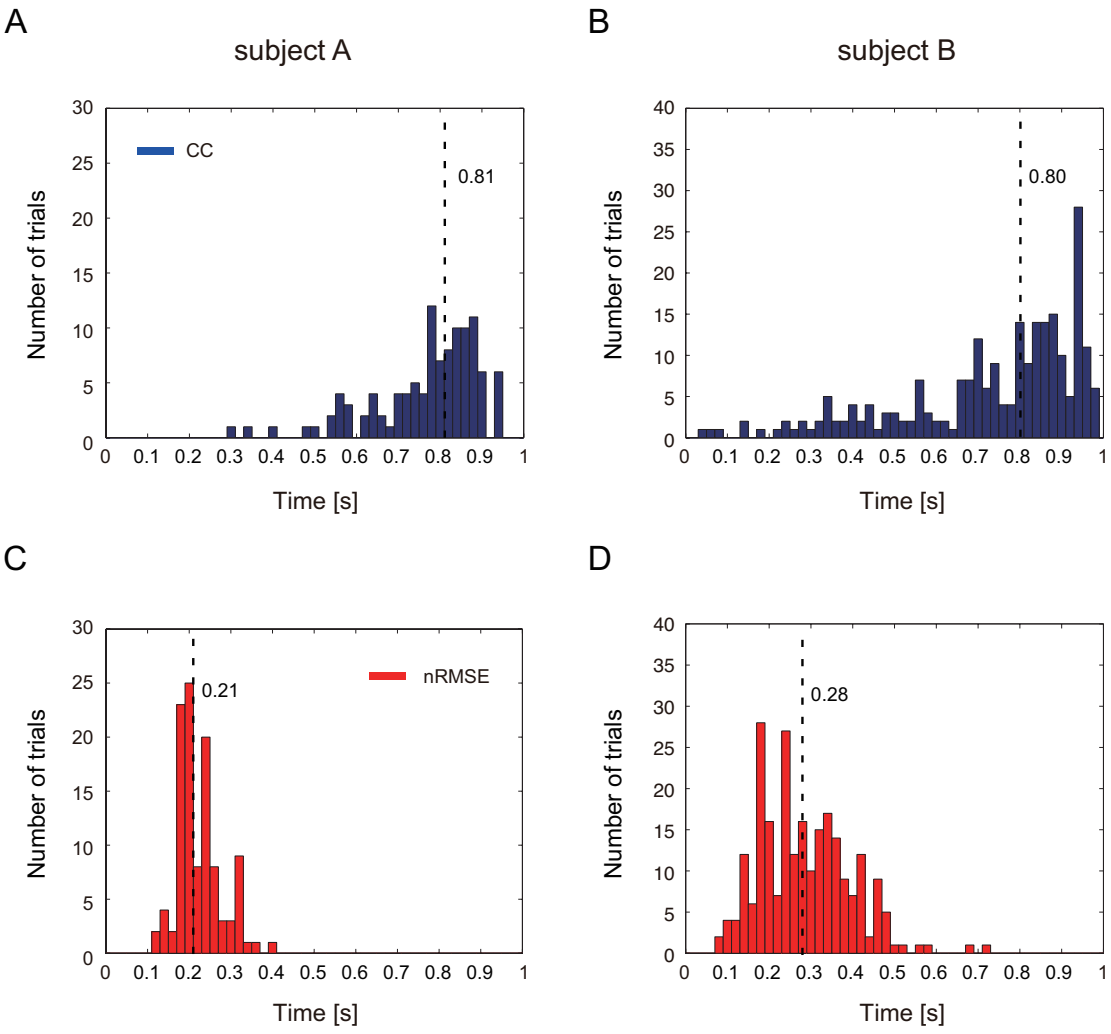

Figure 4-4. Histogram of whole result in 10-fold cross validation

The height of each blue and red bar is equal to the number of trials according to CC and nRMSE, respectively, with density of interval (0.02). The total area of histogram is equal to the whole number of test trials 10-fold cross validation for both monkeys. We noted that, for visualization, all negative CC values were substituted. Dotted line showed the median of CC and nRMSE for both monkeys.

4.3.2 Contribution of individual electrodes and frequency bands to decoding

Figure 4-5 shows the calculated contribution of each electrode to the decoding. For monkey A, the first, second, and third highest contributing electrodes were 7, 9, and 5, respectively. For monkey B, the three highest contributing electrodes were 15, 6, and 5. The contributions of each frequency band were also calculated. The β2 band showed the highest contribution for monkey A, and the γ4 band was highest for monkey B. A two-way ANOVA was applied to analyze the contribution matrix of the 15 or 16 electrodes and the ten frequency bands. No significant difference was observed between the 15 or 16 electrodes of the two monkeys (monkey A: $F_{14, 126} = 1.29$, $p = 0.22$; monkey B: $F_{15, 135} = 1.56$, $p = 0.09$). Significant differences between frequency bands were observed in monkey B, where the γ3 and γ4 bands were significantly higher than the θ, β1, β2 and γ1 bands. Moreover, the γ5 band was significantly higher than the γ1 band (monkey B: $F_{9, 135} = 6.01$, $p = 4.54\times10^{-7}$), as shown in Figure 4-6. For monkey A, no significant difference was observed between frequency bands (monkey A: $F_{9, 126} = 1.88$, $p = 0.06$). In addition, we also decoded grasp force profile using each individual frequency band of the ECoG feature signals to investigate their individual contributions to prediction. The decoding performance (CC) using δ, β1, γ2, γ3, γ4 and frequency bands were significantly higher than using θ, α, β2, γ1, and γ5 frequency bands ($F_{9, 1090} = 40.44$, $p = 1.70\times10^{-62}$, one-way ANOVA with the Tukey-Kramer test) for monkey A. For monkey B, the decoding performance (CC) using δ, γ2, γ3, γ4 and γ5 frequency bands were significantly higher than using θ, α, β1, β2, and γ1 frequency bands ($F_{9,}$

$_{2390}$ = 34.88, p = 2.46×10^{-58}). The γ2, γ3, γ4 showed greater efficacy in both monkeys.

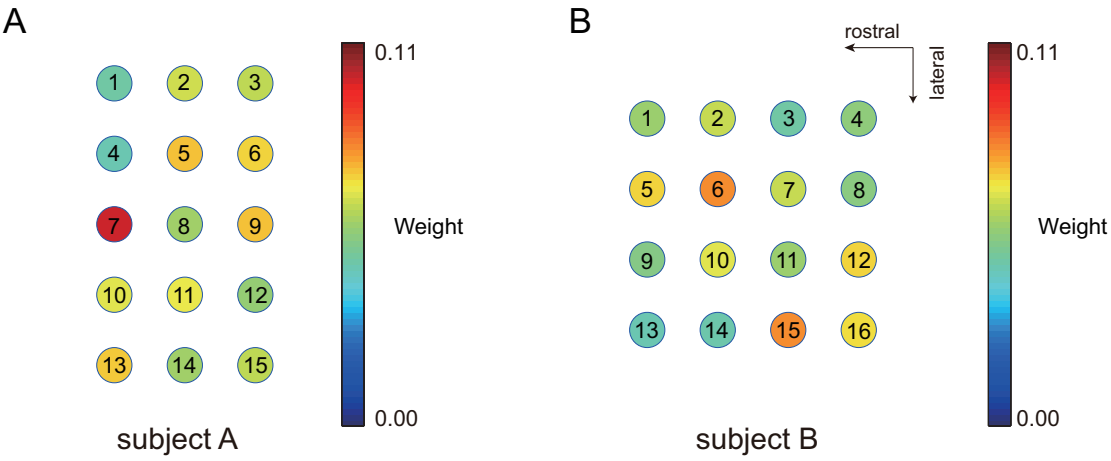

Figure 4-5. Contribution of electrodes

The color mapping of each electrode represents the contribution of that electrode in the prediction model. Contribution values ranged from 0.00 to 0.11 for both monkeys.

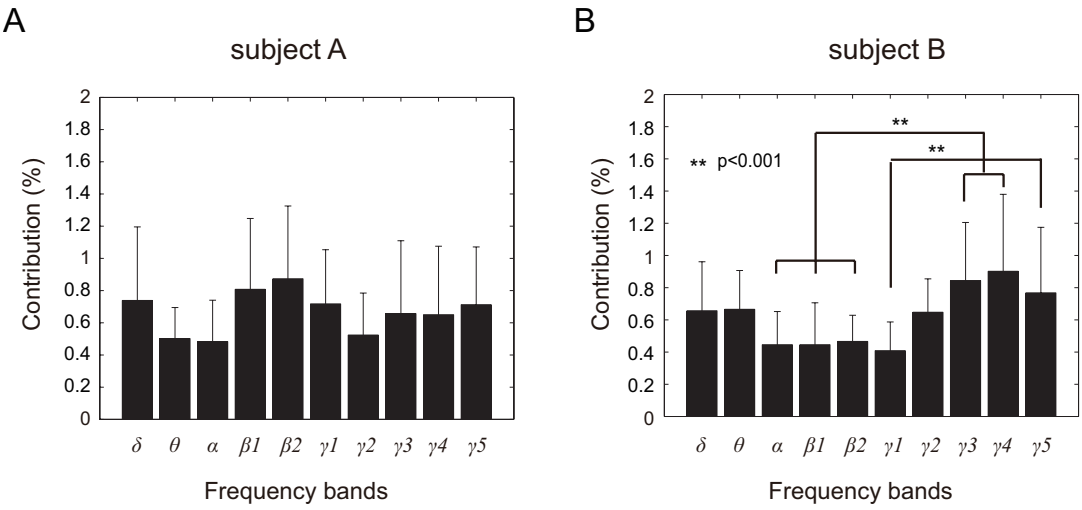

Figure 4-6. Contribution of frequency bands

Each bar represents the contribution of a frequency band in the contribution matrix of electrodes and frequency bands. We performed a two-way ANOVA with contribution of electrodes and frequency bands. Significant differences between weight values of frequency bands are denoted with ** ($p < 0.001$).

4.4 Discussion

In this study, grasp force profiles were successfully decoded from ECoG signals recorded from primary sensorimotor cortex. To the best of our knowledge, this is the first attempt to decode real grasp force profiles from ECoG time series, and sparse linear regression algorithm did not detect irrelevant information of the motor cortex. To the best of our knowledge, this is the first attempt to decode real grasp force profiles from ECoG time series. These results, combined with our previous decoding of hand trajectory (Chen et al., 2013), suggest the feasibility to realize high performance ECoG-based neural prosthetics controllable in multiple degrees of freedoms.

A previous study on electromyography-based finger grasp force decoding (Kamavuako et al., 2013) showed that force can be recorded and predicted precisely with the wrist of the subject fixed during a finger grasping task. However, in a reaching and grasping task, the recorded force data should be considered as a combination of forces rather than a simple finger grasp force, which maybe affected by shoulder, elbow, and wrist joint torque, arm momentum, and other such factors. For these reasons, we decoded the temporal profile of grasp, a principle component of finger dynamics, rather than the absolute value of force data. Further more, grasping force decoding during reaching tasks is more important for real application development than static force decoding because it is natural to occur in our everyday life.

Grasping is a fundamental capability of the hand and a key area for investigating motor function and developing BMIs. It has been shown that neuron activities in

anterior intraparietal cortex (Baumann et al., 2009), dorsal premotor cortex, and primary motor cortex (Mason et al., 2002 and Hendrix et al., 2009) are correlated with target object properties, hand shape, and grasp force level. Furthermore, Carmena et al. (2003) decoded intended grasp force to control grasping by a robot arm. Open and close control (Velliste et al 2008, Hochberg et al., 2012) and aperture decoding and control (Zhuang et al., 2010, Bansal et al., 2011, Bansal et al., 2012, and Collinger et al., 2013) of grippers have also been investigated. Differing from previous studies, in this current work, we decoded grasp force profiles from ECoG time series, presenting a potentially more natural and realistic control method for neural prosthetics.

Early studies investigated finger movements related unit activity in the M1 (Smith et al., 1975, Fetz and Cheney, 1980, and Buys et al., 1986), while long-standing controversy over whether “muscles” or “movements” are represented in the M1 (Kakei et al., 1999). We focused on high-γ component of ECoG, because the high-γ component of LFP or ECoG reflects the spiking activity (Ray et al., 2008, and Yazdan-Shahmorad et al. 2013).

The high gamma bands of ECoG feature signals showed higher amplitude before grasping, and higher amplitude last to time point of peak force in monkey B (Figure 2B). Then, the amplitude decreased. For monkey A (Figure 2A), these trends of ECoG feature data were not clear like monkey B. Analysis of weight values in the decoding models showed that γ3 and γ4 were a significantly effective bands for monkey B. Analysis of individual contribution of each frequency band also revealed that the γ2, γ3, and γ4 bands significantly affected on the contribution

of decoding in both monkeys. These results were consistent with our previous decoding of hand trajectory (Chen et al., 2013), and suggested greater efficacy for high γ bands in decoding multiple motor parameters, while we could not find anatomical evidence about the most effective site for finger force movement in this study.

Chapter 5

Perspective of brain research and interface development with ECoG signals

5.1 Developments of next generational ECoG

With the great achievement in ECoG related research, wireless ECoG electrodes have been developed (Hirata et al., 2011, and Bjorninen et al., 2012). The high density and large-scale ECoG electrodes, which can cover the whole of brain, have been focus as future direction of development of ECoG electrodes.

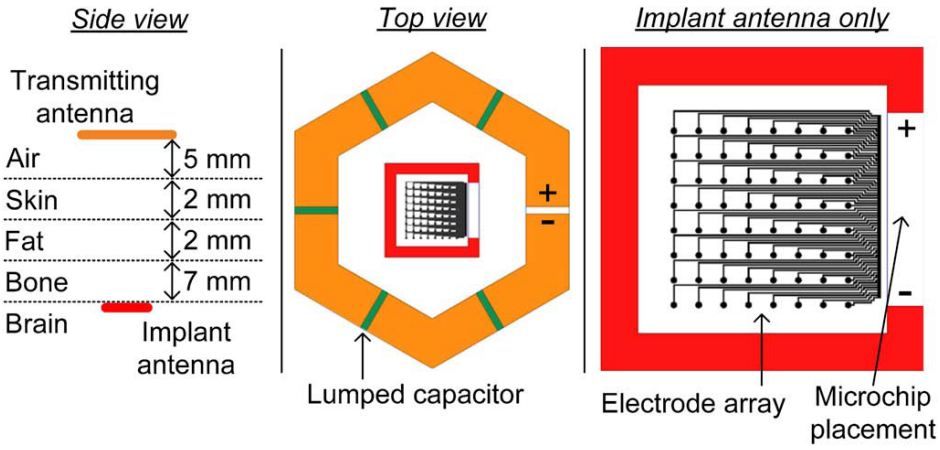

Figure 5-1. Design of wireless ECoG electrode

This figure is from Bjorninen et al., 2012.

5.2 Future brain research with ECoG signals

5.2.1 Major obstacles in brain research

Brain is the central of nervous systems, control over the whole parts of our body and activities, such as movement, thinking and feeling. More than one hundred years,

productive experiments were held, and knowledge have been gotten from different level of brain research, from protein, gene, synapses, cells, microcircuits, brain regions to whole brain, as shown in Figure 5.1. However, proper understanding between different levels of brain is still lacking, for example, the links from neuron spike activities to learning and memory. The major obstacle in brain research is fragmentation of different parts and levels in brain research.

To solve these problems, huge research projects are being held in the world. In Europe, Human Brain research project which aims to simulate the complete human brain on supercomputer to better understand how it functions, involve hundreds of researchers, from 135 partner institutions in 26 countries. Its total costs are estimated at 1.190 billion euro for ten years. In American, Brain Activity Map Project is a proposed collaborative research initiative, with the goal of mapping the activity of every neuron in human brain. The budgets have been projected to cost more than $300 million per year for ten years. A huge national research project also will be held in japan with the aim of elucidating the network of whole brain.

Almost at the same time, the primary countries in the world started huge brain research projects. It suggested the possibility of elucidating the network of whole brain have been the common knowledge among the brain researchers in the world.
The process of these research projects will be the milestone in the history of brain research.

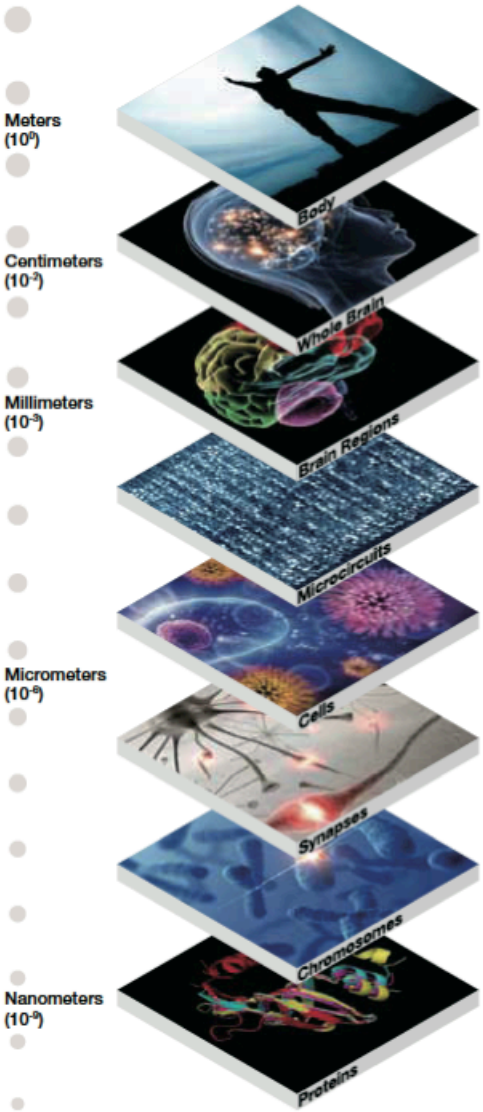

Figure 5-2. From molecules to the body: spatial scales for the brain's different levels of organization span nine orders of magnitude

https://www.humanbrainproject.eu Human Brain Project Report to European Commission

5.2.2 Brain research with next generational ECoG signals

Although the record of single neuron activity is most direct way to investigate network activity and the function of brain, the possible recording number of neurons

still limited in about hundreds. ECoG signals represent the activity of a population of cells. ECoG signals show great potential to investigate real-time network activity, with the development of multi-channel ECoG electrode, which can cover the whole of brain.

This study clearly demonstrated that multiply motor parameters could be decoded from ECoG signals, and the most effective areas for hand trajectory decoding were concentrated at the lateral areas and areas close to the central sulcus (CS), as shown in Figure 5-2. These results gave us the vision of large areas in the brain, which is difficult by using invasive recording methods, because it is very difficult to record neuron activities from large area of brain, simultaneously.

With this advantage, we believe that it is possible to investigate the network activity between different brain areas, builting a bridge across single neuron activity to brain regions in brain research with next generational ECoG signals.

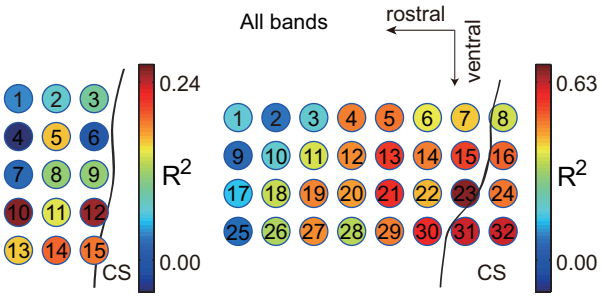

Figure 5-3. Decoding performances with individual ECoG electrodes

The color map in each electrode showed the performance by using this electrode. For monkey A, the R^2 value changed form 0.00 to 0.24. For monkey B, the R^2 value changed form 0.00 to 0.63.

5.3 Future brain machine interface development with ECoG signals

Brain machine interface aims at the restoration of lost function of disable people. Although several laboratory works (Hochberg et al., 2006, Hochberg et al., 2012, and Collinger et al., 2013) showed these developments hold promising, it will be still a long way and it can be applicable in our everyday life. There are also some issues should be discussed in figure brain machine interface.

First of all, we should consider the measurement of brain signals. The ideal measure method for BMI can be fully implanted, and have very long-term recording stability from lager number of neurons from multiple brain areas. In this view, ECoG-based BMIs meet this need well.

Secondly, the computationally efficient algorithms are also needed for real time control. The efficiency of feature selection method and decoding method is important. In this study, band-pass filter, z-score normalization and linear regression method were used in selecting motor related feature and training model. The computational cost of these methods were very low, and suitable for real time processing.

Thirdly, the long-term usage of brain machine interface will change the brain. How to use brain plasticity to incorporate prosthetic devices is still an opening question in the future.

Fourthly, the final goal maybe is to make the prosthetic device feel like the user's own limb using micro-stimulation of cortical sensory areas based on neural feedback function.

Anyway, recent ECoG based works have showed the long-term stability of ECOG signals (Chao et al., 2010), discussed the location of ECoG electrodes, subdural (Chao et al., 2010) and epidural (Shimoda et al., 2012), investigated the necessary number of ECoG electrodes and most efficient areas of ECoG recording (Chen et al., 2013). Combined with wireless system of ECOG signals (Hirata et al., 2011, and Bjorninen et al., 2012), ECoG signals hold promising in developing high performance neural prosthetics controllable in the future.

Chapter 6

Conclusion

6.1 Summary

The motivation of this thesis is to develop a new type of upper limb brain machine interface for practical application. To accomplish it, the background of brain machine interface was investigated, including invasive, noninvasive brain machine interface. Since the high clinical risk in invasive methods, and the low information capacity in noninvasive methods, ECoG signals were selected as signals source for relatively low invasiveness and high spatial-temporal resolution.

To complete a neural prosthetic with multi-degree of freedom, position in formation and control method for gripping is necessary. Thus, we intended to decode hand trajectory and force information from ECoG signals. Two monkeys were trained to perform reaching and grasping task. The ECoG signals, 3D hand positions and grasp force were recorded simultaneously during behavioral task.

We proposed an algorithm to decode hand trajectory and grasp force from 15 and 32 channel ECoG signals recorded from primary motor cortex (M1) in two primates. To determine the most effective areas for prediction, we applied two electrode selection methods, one based on position relative to the central sulcus (CS) and another based on the electrodes' individual prediction performance. The best coefficients of determination for decoding hand trajectory in the two monkeys were

0.4815 ± 0.0167 and 0.7780 ± 0.0164. Performance results from individual ECoG electrodes showed that those with higher performance were concentrated at the lateral areas and areas close to the CS. The results of prediction according with different numbers of electrodes based on proposed methods were also shown and discussed. These results also suggest that superior decoding performance can be achieved from a group of effective ECoG signals rather than an entire ECoG array.

We also demonstrated that lateral grasp force profile can be decoded using a sparse linear regression from 15 and 16 channel ECoG signals recorded from sensorimotor cortex in two non-human primates. The best average correlation coefficients of prediction after 10-fold cross validation were 0.82 ± 0.09 and 0.79 ± 0.15 for our monkeys A and B, respectively. These results show that grasp force profile was successfully decoded from ECoG signals in reaching and grasping tasks and may potentially contribute to the development of more natural control methods for grasping in neural prosthetics.

In addition, the future directions of brain research and interface development were investigated. The major burns in current brain research and interface development were discussed. With the development of next generational ECoG electrode, ECoG signals may play an important role in future brain and interface research.

6.2 Future work

As future work, we want to complete real time robot control. An open loop control is possible to complete based on the result mentioned about. The main parts of open loop control can be divided into three parts: the starting time point of reaching and grasping, target hand trajectory of robot arm, and control of gripper.

In previous ECoG based study, the starting time point of reaching and grasping were decoded successfully (Pistol et al., 2013). It is possible to achieve the same result. For target hand trajectory of robot arm, we can predict the target hand trajectory from ECoG signals (Chen et al., 2013). Then, shoulder and elbow joint angle can be calculated based on the predicted hand trajectory and length of robot arm (Koike et al., 2013). It is in discussion whether open or closed loop control method is better. We also want to decode aperture, the distant between thumb and index finger, from ECoG signals because aperture control of gripper is usual control method in current control systems (Zhuang et al., 2010, Bansal et al., 2011, Bansal et al., 2012, and Collinger et al., 2013). In addition, force control of the gripper during grasping will be held based on the predicted grasp force profile (Chen et al., 2013).

In addition, to develop a more compatible brain machine interface, the interaction between the monkey and physical world should be investigated. New system also should make use of the learning ability of monkey and the plasticity of brain. In this study, the monkeys were trained to perform reaching and grasping task only. Additional task were not investigated. In needle-based search (Velliste et al., 2008), it had been suggested that the monkeys learned to control robot arm with multi-degree of freedom to perform some movement, which is not necessary to self-feeding task and an assisted brain-controlled task is useful and an important phase for the monkeys to learn the robot arm by their neuron activities purely in the end. The plasticity of neuron activities and brain in this process may be very important to investigate how the brain learn and control a device outside directly. For ECoG signals, how to design an assisted brain-controlled task, whether the monkey can adapt neuron activity to

control the robot with ECoG signals, because ECoG signals reflect the population activity of brain rather than single neuron activity, and if they can, whether the plasticity of neuron activities with ECoG signal is the same with the plasticity of single neuron activity, are still opening question for future research.

Reference

Acharya, S., Fifer, M.S., Benz, H.L., Crone, N.E., Thakor, N.V., 2010. Electrocorticographic amplitude predicts finger positions during slow grasping motions of the hand. Journal of Neural Engineering 7.

Aggarwal, V., Acharya, S., Tenore, F., Shin, H.C., Etienne-Cummings, R., Schieber, M.H., Thakor, N.V., 2008. Asynchronous decoding of dexterous finger movements using M1 neurons. Ieee Transactions on Neural Systems and Rehabilitation Engineering 16, 3-14.

Bansal, A.K., Truccolo, W., Vargas-Irwin, C.E., Donoghue, J.P., 2012. Decoding 3D reach and grasp from hybrid signals in motor and premotor cortices: spikes, multiunit activity, and local field potentials. Journal of Neurophysiology 107, 1337-1355.

Bansal, A.K., Vargas-Irwin, C.E., Truccolo, W., Donoghue, J.P., 2011. Relationships among low-frequency local field potentials, spiking activity, and three-dimensional reach and grasp kinematics in primary motor and ventral premotor cortices. Journal of Neurophysiology 105, 1603-1619.

Baumann, M.A., Fluet, M.C., Scherberger, H., 2009. Context-Specific Grasp Movement Representation in the Macaque Anterior Intraparietal Area. Journal of Neuroscience 29, 6436-6448.

Birbaumer, N., Ghanayim, N., Hinterberger, T., Iversen, I., Kotchoubey, B., Kubler, A., Perelmouter, J., Taub, E., Flor, H., 1999. A spelling device for the paralysed. Nature 398, 297-298.

Bjorninen, T., Muller, R., Ledochowitsch, P., Sydanheimo, L., Ukkonen, L., Maharbiz, M.M., Rabaey, J.M., 2012. Design of Wireless Links to Implanted Brain-Machine Interface Microelectronic Systems. Ieee Antennas and Wireless Propagation Letters 11, 1663-1666.

Buys, E.J., Lemon, R.N., Mantel, G.W.H., Muir, R.B., 1986. Selective Facilitation of Different Hand Muscles by Single Corticospinal Neurons in the Conscious Monkey. Journal of Physiology-London 381, 529-549.

Carmena, J.M., Lebedev, M.A., Crist, R.E., O'Doherty, J.E., Santucci, D.M., Dimitrov, D.F., Patil, P.G., Henriquez, C.S., Nicolelis, M.A.L., 2003. Learning to control a brain-machine interface for reaching and grasping by primates. Plos Biology 1, 193-208.

Chapin, J.K., Moxon, K.A., Markowitz, R.S., Nicolelis, M.A.L., 1999. Real-time control of a robot arm using simultaneously recorded neurons in the motor cortex. Nature Neuroscience 2, 664-670.

Chao, Z.C., Nagasaka, Y., Fujii, N., 2010. Long-term asynchronous decoding of arm motion using electrocorticographic signals in monkeys. Front Neuroeng 3, 3.

Chestek, C.A., Gilja, V., Blabe, C.H., Foster, B.L., Shenoy, K.V., Parvizi, J., Henderson, J.M., 2013. Hand posture classification using electrocorticography signals in the gamma band over human sensorimotor brain areas. Journal of Neural Engineering 10.

Chin, C.M., Popovic, M.R., Thrasher, A., Cameron, T., Lozano, A., Chen, R., 2007. Identification of arm movements using correlation of electrocorticographic spectral components and kinematic recordings. Journal of Neural Engineering 4, 146-158.

Collinger, J.L., Wodlinger, B., Downey, J.E., Wang, W., Tyler-Kabara, E.C., Weber, D.J., McMorland, A.J.C., Velliste, M., Boninger, M.L., Schwartz, A.B., 2013. High-performance neuroprosthetic control by an individual with tetraplegia. Lancet 381, 557-564.

Ethier, C., Oby, E.R., Bauman, M.J., Miller, L.E., 2012. Restoration of grasp following paralysis through brain-controlled stimulation of muscles. Nature 485, 368-371.

Fagg, A.H., Hatsopoulos, N.G., de Lafuente, V., Moxon, K.A., Nemati, S., Rebesco, J.M., Romo, R., Solla, S.A., Reimer, J., Tkach, D., Pohlmeyer, E.A., Miller, L.E., 2007. Biomimetic brain machine interfaces for the control of movement. Journal of Neuroscience 27, 11842-11846.

Fetz, E.E., Cheney, P.D., 1980. Postspike Facilitation of Forelimb Muscle-Activity by Primate Corticomotoneuronal Cells. Journal of Neurophysiology 44, 751-772.

Ganesh, G., Burdet, E., Haruno, M., Kawato, M., 2008. Sparse linear regression for reconstructing muscle activity from human cortical fMRI. Neuroimage 42, 1463-1472.

Ganguly, K., Dimitrov, D.F., Wallis, J.D., Carmena, J.M., 2011. Reversible large-scale modification of cortical networks during neuroprosthetic control. Nature Neuroscience 14, 662-U164.

Geladi, P., Kowalski, B.R., 1986. Partial Least-Squares Regression - a Tutorial. Analytica Chimica Acta 185, 1-17.

Gilja, V., Nuyujukian, P., Chestek, C.A., Cunningham, J.P., Yu, B.M., Fan, J.M., Churchland, M.M., Kaufman, M.T., Kao, J.C., Ryu, S.I., Shenoy, K.V., 2012. A high-performance neural prosthesis enabled by control algorithm design. Nature Neuroscience 15, 1752-1757.

Griffin, D.M., Hudson, H.M., Belhaj-Saif, A., McKiernan, B.J., Cheney, P.D., 2008. Do corticomotoneuronal cells predict target muscle EMG activity? Journal of Neurophysiology 99, 1169-1186.

Hadjidimitriou, S.K., Hadjileontiadis, L.J., 2012. Toward an EEG-Based Recognition of Music Liking Using Time-Frequency Analysis. Ieee Transactions on Biomedical Engineering 59, 3498-3510.

Hao, Y.Y., Zhang, Q.S., Zhang, S.M., Zhao, T., Wang, Y.W., Chen, W.D., Zheng, X.X., 2013. Decoding grasp movement from monkey premotor cortex for real-time prosthetic hand control. Chinese Science Bulletin 58, 2512-2520.

Hauschild, M., Mulliken, G.H., Fineman, I., Loeb, G.E., Andersen, R.A., 2012. Cognitive signals for brain-machine interfaces in posterior parietal cortex include continuous 3D trajectory commands. Proceedings of the National Academy of Sciences of the United States of America 109, 17075-17080.

Hendrix, C.M., Mason, C.R., Ebner, T.J., 2009. Signaling of Grasp Dimension and Grasp Force in Dorsal Premotor Cortex and Primary Motor Cortex Neurons During Reach to Grasp in the Monkey. Journal of Neurophysiology 102, 132-145.

Hirata, M., Matsushita, K., Suzuki, T., Yoshida, T., Sato, F., Morris, S., Yanagisawa, T., Goto, T., Kawato, M., Yoshimine, T., 2011. A Fully-Implantable Wireless System for Human Brain-Machine Interfaces Using Brain Surface Electrodes: W-HERBS. Ieice Transactions on Communications E94b, 2448-2453.

Hochberg, L.R., Bacher, D., Jarosiewicz, B., Masse, N.Y., Simeral, J.D., Vogel, J., Haddadin, S., Liu, J., Cash, S.S., van der Smagt, P., Donoghue, J.P., 2012. Reach and grasp by people with tetraplegia using a neurally controlled robotic arm. Nature 485, 372-U121.

Hochberg, L.R., Serruya, M.D., Friehs, G.M., Mukand, J.A., Saleh, M., Caplan, A.H., Branner, A., Chen, D., Penn, R.D., Donoghue, J.P., 2006. Neuronal ensemble control of prosthetic devices by a human with tetraplegia. Nature 442, 164-171.

Kakei, S., Hoffman, D.S., Strick, P.L., 1999. Muscle and movement representations in the primary motor cortex. Science 285, 2136-2139.

Kamavuako, E.N., Rosenvang, J.C., Bog, M.F., Smidstrup, A., Erkocevic, E., Niemeier, M.J., Jensen, W., Farina, D., 2013. Influence of the feature space on the estimation of hand grasping force from intramuscular EMG. Biomedical Signal Processing and Control 8, 1-5.

Kellis, S., Miller, K., Thomson, K., Brown, R., House, P., Greger, B., 2010. Decoding spoken words using local field potentials recorded from the cortical surface. Journal of Neural Engineering 7.

Koike, Y., Hirose, H., Sakurai, Y., Iijima, T., 2006. Prediction of arm trajectory from a small number of neuron activities in the primary motor cortex. Neuroscience Research 55, 146-153.

Koralek, A.C., Jin, X., Ii, J.D.L., Costa, R.M., Carmena, J.M., 2012. Corticostriatal plasticity is necessary for learning intentional neuroprosthetic skills. Nature 483, 331-335.

Krishnan, A., Williams, L.J., McIntosh, A.R., Abdi, H., 2011. Partial Least Squares (PLS) methods for neuroimaging: A tutorial and review. Neuroimage 56, 455-475.

Kubanek, J., Miller, K.J., Ojemann, J.G., Wolpaw, J.R., Schalk, G., 2009. Decoding flexion of individual fingers using electrocorticographic signals in humans. Journal of Neural Engineering 6.

Lebedev, M.A., Carmena, J.M., O'Doherty, J.E., Zacksenhouse, M., Henriquez, C.S., Principe, J.C., Nicolelis, M.A.L., 2005. Cortical ensemble adaptation to represent velocity of an artificial actuator controlled by a brain-machine interface. Journal of Neuroscience 25, 4681-4693.

Ludwig, K.A., Miriani, R.M., Langhals, N.B., Joseph, M.D., Anderson, D.J., Kipke, D.R., 2009. Using a Common Average Reference to Improve Cortical Neuron Recordings From Microelectrode Arrays. Journal of Neurophysiology 101, 1679-1689.

Mason, C.R., Gomez, J.E., Ebner, T.J., 2002. Primary motor cortex neuronal discharge during reach-to-grasp: Controlling the hand as a unit. Archives Italiennes De Biologie 140, 229-236.

McFarland, D.J., McCane, L.M., David, S.V., Wolpaw, J.R., 1997. Spatial filter selection for EEG-based communication. Electroencephalography and Clinical Neurophysiology 103, 386-394.

Morrow, M.M., Miller, L.E., 2003. Prediction of muscle activity by populations of sequentially recorded primary motor cortex neurons. Journal of Neurophysiology 89, 2279-2288.

Musallam, S., Corneil, B.D., Greger, B., Scherberger, H., Andersen, R.A., 2004. Cognitive control signals for neural prosthetics. Science 305, 258-262.

Nakanishi, Y., Yanagisawa, T., Shin, D., Fukuma, R., Chen, C., Kambara, H., Yoshimura, N., Hirata, M., Yoshimine, T., Koike, Y., 2013. Prediction of Three-Dimensional Arm Trajectories Based on ECoG Signals Recorded from Human Sensorimotor Cortex. Plos One 8.

Nambu, I., Osu, R., Sato, M.A., Ando, S., Kawato, M., Naito, E., 2009. Single-trial reconstruction of finger-pinch forces from human motor-cortical activation measured by near-infrared spectroscopy (NIRS). Neuroimage 47, 628-637.

Neal RM., Bayesian learning for neural networks. 1996. Lect. Notes Stat. No. 118. New York: Springer-Verlag.

Pistohl, T., Schmidt, T.S.B., Ball, T., Schulze-Bonhage, A., Aertsen, A., Mehring, C., 2013. Grasp Detection from Human ECoG during Natural Reach-to-Grasp Movements. Plos One 8.

Pistohl, T., Schulze-Bonhage, A., Aertsen, A., Mehring, C., Ball, T., 2012. Decoding natural grasp types from human ECoG. Neuroimage 59, 248-260.

Ray, S., Crone, N.E., Niebur, E., Franaszczuk, P.J., Hsiao, S.S., 2008. Neural Correlates of High-Gamma Oscillations (60-200 Hz) in Macaque Local Field Potentials and Their Potential Implications in Electrocorticography. Journal of Neuroscience 28, 11526-11536.

Rathelot, J.A., Strick, P.L., 2009. Subdivisions of primary motor cortex based on cortico-motoneuronal cells. Proceedings of the National Academy of Sciences of the United States of America 106, 918-923.

Rickert, J., de Oliveira, S.C., Vaadia, E., Aertsen, A., Rotter, S., Mehring, C., 2005. Encoding of movement direction in different frequency ranges of motor cortical local field potentials. Journal of Neuroscience 25, 8815-8824.

Rosipal, R., Kramer, N., 2006. Overview and recent advances in partial least squares. Subspace, Latent Structure and Feature Selection 3940, 34-51.

Sanchez, J.C., Carmena, J.M., Lebedev, M.A., Nicolelis, M.A.L., Harris, J.G., Principe, J.C., 2004. Ascertaining the importance of neurons to develop better brain-machine interfaces. Ieee Transactions on Biomedical Engineering 51, 943-953.

Sato, M., 2001. Online model selection based on the variational bayes. Neural Computation 13, 1649-1681.

Schalk, G., Kubanek, J., Miller, K.J., Anderson, N.R., Leuthardt, E.C., Ojemann, J.G., Limbrick, D., Moran, D., Gerhardt, L.A., Wolpaw, J.R., 2007. Decoding two-dimensional movement trajectories using electrocorticographic signals in humans. Journal of Neural Engineering 4, 264-275.

Schalk, G., Miller, K.J., Anderson, N.R., Wilson, J.A., Smyth, M.D., Ojemann, J.G., Moran, D.W., Wolpaw, J.R., Leuthardt, E.C., 2008. Two-dimensional movement control using electrocorticographic signals in humans. Journal of Neural Engineering 5, 75-84.

Shibata, K., Watanabe, T., Sasaki, Y., Kawato, M., 2011. Perceptual Learning Incepted by Decoded fMRI Neurofeedback Without Stimulus Presentation. Science 334, 1413-1415.

Shimoda, K., Nagasaka, Y., Chao, Z.C., Fujii, N., 2012. Decoding continuous three-dimensional hand trajectories from epidural electrocorticographic signals in Japanese macaques. Journal of Neural Engineering 9.

Shin, D., Watanabe, H., Kambara, H., Nambu, A., Isa, T., Nishimura, Y., Koike, Y., 2012. Prediction of Muscle Activities from Electrocorticograms in Primary Motor Cortex of Primates. Plos One 7.

Smith, A.M., Heppreymond, M.C., Wyss, U.R., 1975. Relation of Activity in Precentral Cortical-Neurons to Force and Rate of Force Change during Isometric Contractions of Finger Muscles. Experimental Brain Research 23, 315-332.

Tankus, A., Fried, I., Shoham, S., 2012. Sparse decoding of multiple spike trains for brain-machine interfaces. Journal of Neural Engineering 9.

Taylor, D.M., Tillery, S.I.H., Schwartz, A.B., 2002. Direct cortical control of 3D neuroprosthetic devices. Science 296, 1829-1832.

Ting, J.A., D'Souza, A., Yamamoto, K., Yoshioka, T., Hoffman, D., Kakei, S., Sergio, L., Kalaska, J., Kawato, M., Strick, P., Schaal, S., 2008. Variational Bayesian least squares: an application to brain-machine interface data. Neural Netw 21, 1112-1131.

Toda, A., Imamizu, H., Kawato, M., Sato, M.A., 2011. Reconstruction of two-dimensional movement trajectories from selected magnetoencephalography cortical currents by combined sparse Bayesian methods. Neuroimage 54, 892-905.

Thulasidas, M., Guan, C., Wu, J.K., 2006. Robust classification of EEG signal for brain-computer interface. Ieee Transactions on Neural Systems and Rehabilitation Engineering 14, 24-29.

Velliste, M., Perel, S., Spalding, M.C., Whitford, A.S., Schwartz, A.B., 2008. Cortical control of a prosthetic arm for self-feeding. Nature 453, 1098-1101.

Wang, W., Collinger, J.L., Degenhart, A.D., Tyler-Kabara, E.C., Schwartz, A.B., Moran, D.W., Weber, D.J., Wodlinger, B., Vinjamuri, R.K., Ashmore, R.C., Kelly, J.W., Boninger, M.L., 2013. An Electrocorticographic Brain Interface in an Individual with Tetraplegia. Plos One 8.

Watanabe, H., Sato, M., Suzuki, T., Nambu, A., Nishimura, Y., Kawato, M., Isa, T., 2012. Reconstruction of movement-related intracortical activity from micro-electrocorticogram array signals in monkey primary motor cortex. Journal of Neural Engineering 9.

Wessberg, J., Stambaugh, C.R., Kralik, J.D., Beck, P.D., Laubach, M., Chapin, J.K., Kim, J., Biggs, J., Srinivasan, M.A., Nicolelis, M.A.L., 2000. Real-time prediction of hand trajectory by ensembles of cortical neurons in primates. Nature 408, 361-365.

Wilson, J.A., Felton, E.A., Garell, P.C., Schalk, G., Williams, J.C., 2006. ECoG factors underlying multimodal control of a brain-computer interface. Ieee Transactions on Neural Systems and Rehabilitation Engineering 14, 246-250.

Wold, S., Ruhe, A., Wold, H., Dunn, W.J., 1984. The Collinearity Problem in Linear-Regression - the Partial Least-Squares (Pls) Approach to Generalized Inverses. Siam Journal on Scientific and Statistical Computing 5, 735-743.

Wolpaw, J.R., McFarland, D.J., 2004. Control of a two-dimensional movement signal by a noninvasive brain-computer interface in humans. Proceedings of the National Academy of Sciences of the United States of America 101, 17849-17854.

Wolpaw, J.R., Mcfarland, D.J., Neat, G.W., Forneris, C.A., 1991. An Eeg-Based Brain-Computer Interface for Cursor Control. Electroencephalography and Clinical Neurophysiology 78, 252-259.

Yanagisawa, T., Hirata, M., Saitoh, Y., Goto, T., Kishima, H., Fukuma, R., Yokoi, H., Kamitani, Y., Yoshimine, T., 2011. Real-time control of a prosthetic hand using human electrocorticography signals. Journal of Neurosurgery 114, 1715-1722.

Yanagisawa, T., Hirata, M., Saitoh, Y., Kato, A., Shibuya, D., Kamitani, Y., Yoshimine, T., 2009. Neural decoding using gyral and intrasulcal electrocorticograms. Neuroimage 45, 1099-1106.

Yanagisawa, T., Hirata, M., Saitoh, Y., Kishima, H., Matsushita, K., Goto, T., Fukuma, R., Yokoi, H., Kamitani, Y., Yoshimine, T., 2012. Electrocorticographic Control of a Prosthetic Arm in Paralyzed Patients. Annals of Neurology 71, 353-361.

Yoshimura, N., Dasalla, C.S., Hanakawa, T., Sato, M.A., Koike, Y., 2012. Reconstruction of flexor and extensor muscle activities from electroencephalography cortical currents. Neuroimage 59, 1324-1337.

Zhuang, J., Truccolo, W., Vargas-Irwin, C., Donoghue, J.P., 2010. Decoding 3-D Reach and Grasp Kinematics From High-Frequency Local Field Potentials in Primate Primary Motor Cortex. Ieee Transactions on Biomedical Engineering 57, 1774-1784.

Research achievement

Publications in Refereed Journals

1. **Chao Chen**, Duk Shin, Hidenori Watanabe, Yasuhiko Nakanishi, Hiroyuki Kambara, Natsue Yoshimura, Atsushi Nambu, Tadashi Isa, Yukio Nishimura, Yasuharu Koike. Decoding grasp force profile from electrocorticography signals in non-human primate sensorimotor cortex. Neuroscience research 83: 1-7. 2014. **E-published**

2. **Chao Chen**, Duk Shin, Hidenori Watanabe, Yasuhiko Nakanishi, Hiroyuki Kambara, Natsue Yoshimura, Atsushi Nambu, Tadashi Isa, Yukio Nishimura, Yasuharu Koike. Prediction of hand trajectory from electrocorticography signals in primary motor cortex. PLoS ONE 8(12): e83534. 2013.

3. Yasuhiko Nakanishi, Takufumi Yanagisawa, Duk Shin, Ryohei Fukuma, **Chao Chen**, Hiroyuki Kambara, Natsue Yoshimura, Masayuki Hirata, Toshiki Yoshimine, Yasuharu Koike. Prediction of three-dimensional arm trajectories based on ECoG signals recorded from human sensorimotor cortex. PLoS ONE 8(8): e72085. 2013.

4. Yasuhiko Nakanishi, Takufumi Yanagisawa, Duk Shin, **Chao Chen**, Hiroyuki Kambara, Natsue Yoshimura, Ryohei Fukuma, Haruhiko Kishima, Masayuki Hirata, Yasuharu Koike. Decoding three dimensional fingertip motion from electrocorticographic signals in humans. Neuroscience research. 2014. **Accepted**

5. Duk Shin, Yasuhiko Nakanishi, Hiroyuki Kambara, **Chao Chen**, Natsue Yoshimura, Yasuharu Koike: Decoding of Kinetic and Kinematic Information from Electrocorticograms in Sensorimotor Cortex. International Journal of Neurorehabilitation. 2014. **Accepted**.

International conferences

1. **Chao Chen**, Duk Shin, Yasuhiko Nakanishi, Hiroyuki Kambara, Natsue Yoshimura, Hidenori Watanabe, Atsushi Nambu, Tadashi Isa, Yukio Nishimura, Yasuharu Koike. Decoding of arm movement from electrocorticographic signals in primary motor cortex in primates. Neuro2013, Kyoto, Japan. 2013.6

2. **Chao Chen**, Duk Shin, Yasuhiko Nakanishi, Hiroyuki Kambara, Natsue Yoshimura, Hidenori Watanabe, Atsushi Nambu, Tadashi Isa, Yukio Nishimura, Yasuharu Koike. Prediction of hand trajectory from electrocorticogram in primates. SNR2013. Saitama, Japan. 2013.3

3. **Chao Chen**, Duk Shin, Yasuhiko Nakanishi, Hiroyuki Kambara, Natsue Yoshimura, Yasuharu Koike. Prediction of arm movement from electrocorticogram. IEEE EDS wimnact 37. Tokyo, Japan. 2013.2

4. Duk Shin, **Chao Chen**, Yasuhiko Nakanishi, Hiroyuki Kambara, Natsue Yoshimura, Hidenori Watanabe, Atsushi Nambu, Tadashi Isa，Yukio Nishimura, Yasuharu Koike. Prediction of joint angle from muscle activities decoded from electrocorticograms. ISHF2013. Vancouver, B.C., Canada. 2013.6

5. Yasuhiko Nakanishi, Takufumi Yanagisawa, Duk Shin, **Chao Chen**, Hiroyuki Kambara, Natsue Yoshimura, Masayuki Hirata, Toshiki Yoshimine, Yasuharu Koike. Prediction of arm 3D- trajectories from human electrocorticograms. ISHF2013. Vancouver, B.C., Canada. 2013.6

6. Duk Shin, Yasuhiko Nakanishi, **Chao Chen**, Hiroyuki Kambara, Natsue Yoshimura, Hidenori Watanabe, Atsushi Nambu, Tadashi Isa, Yukio Nishimura and Yasuharu Koike. Prediction of Joint angle from decoded Muscle Activities from Electrocorticograms in Primary Motor Cortex, Neuro 2013, Kyoto, Japan. 2013.6

7. Yasuhiko Nakanishi, Takafumi Yanagisawa, Masayuki Hirata, **Chao Chen**, Duk Shin, Toshiki Yoshimine and Yasuharu Koike. Prediction of three-dimensional arm trajectory using ECoG signals in patient's cortical cortex, Neuro 2013, Kyoto, Japan. 2013.6